

“Bayesian calibration of the Mg/Ca paleothermometer in planktic foraminifera”

Jessica E. Tierney¹, Steven B. Malevich¹, William Gray², Lael Vetter¹ & Kaustubh Thirumalai¹

¹University of Arizona, Department of Geosciences, 1040 4th St. Tucson, AZ 85721.

²Laboratoire des Sciences du Climat et de l'Environnement (LSCE/IPSL), Gif-sur-Yvette,
France

This is a post print of a paper published in the journal *Paleoceanography and Paleoclimatology*,

doi: 10.1029/2019PA003744

<https://doi.org/10.1029/2019PA003744>

1 **Bayesian calibration of the Mg/Ca paleothermometer**
2 **in planktic foraminifera**

3 **Jessica E. Tierney¹, Steven B. Malevich¹, William Gray², Lael Vetter¹ &**
4 **Kaustubh Thirumalai¹**

5 ¹University of Arizona Department of Geosciences, 1040 E 4th St Tucson AZ 85721

6 ²Laboratoire des Sciences du Climat et de l'Environnement (LSCE/IPSL), Gif-sur-Yvette, France

7 **Key Points:**

- 8 • We introduce Mg/Ca Bayesian calibrations for planktic foraminifera
9 • Hierarchical modeling is used to constrain multivariate Mg/Ca sensitivities
10 • For deep-time applications, we incorporate estimates of Mg/Ca of seawater

Abstract

The Mg/Ca ratio of planktic foraminifera is a widely-used proxy for sea-surface temperature, but is also sensitive to other environmental factors. Previous work has relied on correcting Mg/Ca for non-thermal influences. Here, we develop a set of Bayesian models for Mg/Ca in four major planktic groups – *Globigerinoides ruber* (including both pink and white chromotypes), *Trilobatus sacculifer*, *Globigerina bulloides*, and *Neogloboquadrina pachyderma* (including *N. incompta*) – that account for the multivariate influences on this proxy in an integrated framework. We use a hierarchical model design that leverages information from both laboratory culture studies and globally-distributed core top data, allowing us to include environmental sensitivities that are poorly constrained by core top observations alone. For applications over longer geological timescales, we develop a version of the model that incorporates changes in the Mg/Ca ratio of seawater. We test our models – collectively referred to as BAYMAG – on sediment trap data and on representative paleoclimate time series and demonstrate good agreement with observations and independent SST proxies. BAYMAG provides probabilistic estimates of past temperatures that can accommodate uncertainties in other environmental influences, enhancing our ability to interpret signals encoded in Mg/Ca.

Plain Language Summary

The amount of magnesium (Mg) incorporated into the calcite shells of tiny protists called foraminifera is determined by the temperature of the water in which they grew. This allows paleoclimatologists to measure the magnesium-to-calcium (Mg/Ca) ratio of fossil foraminiferal shells and determine how past sea-surface temperatures (SSTs) have changed. However, other factors can influence Mg/Ca, like the salinity and pH of seawater. Here, we develop Bayesian models of foraminiferal Mg/Ca that account for all of the influences on Mg/Ca and show how we can use these to improve our interpretations of Mg/Ca data.

1 Introduction

The magnesium-to-calcium (Mg/Ca) ratio of planktic foraminifera is a commonly-used proxy method for reconstructing past sea-surface temperatures (SSTs). It has played a pivotal role informing our understanding of tropical climate dynamics in the Late Quaternary (Lea et al., 2000, 2003; Rosenthal et al., 2003; Stott et al., 2007) as well as in deeper geologic time (e.g., Evans et al., 2018). The proxy has theoretical basis in thermodynamics, which predicts a non-linear increase in Mg incorporation into calcite as temperatures rise (Oomori et al., 1987). Laboratory culturing of planktic foraminifera confirms an exponential dependence of Mg/Ca on temperature, albeit with a stronger sensitivity than thermodynamic predictions, indicating that biological “vital effects” also play a role (Nürnberg et al., 1996; Lea et al., 1999). Laboratory experiments also demonstrate that Mg/Ca in foraminifera is sensitive to other environmental factors, such as salinity and pH (Lea et al., 1999; Kiskirek et al., 2008; Dueñas-Bohórquez et al., 2009; Hönisch et al., 2013; Evans, Wade, et al., 2016). The extent to which these secondary factors compromise SST prediction from Mg/Ca is an ongoing topic of investigation (Ferguson et al., 2008; Mathien-Blard & Bassinot, 2009; J. Arbuszewski et al., 2010; Hönisch et al., 2013; Evans, Wade, et al., 2016; Gray et al., 2018; Gray & Evans, 2019). Beyond competing environmental factors, the depositional environment also influences Mg/Ca. If the calcite saturation state of the bottom waters is low, partial dissolution of foraminiferal calcite occurs, lowering Mg/Ca (Brown & Elderfield, 1996; Rosenthal et al., 2000; Regenberg et al., 2006, 2014).

Previous calibrations for Mg/Ca have been based on either laboratory culturing experiments (Nürnberg et al., 1996; Lea et al., 1999; Gray & Evans, 2019), sediment trap data (Anand et al., 2003; Gray et al., 2018) or modern core tops (Elderfield & Ganssen,

2000; Dekens et al., 2002; Khider et al., 2015; Saenger & Evans, 2019). Culture experiments provide precise constraints on environmental sensitivities, but are limited in that laboratory conditions are not perfect analogs for the natural environment. Sediment traps have an advantage in that seasonality of foraminiferal occurrence and corresponding ocean temperatures are well-constrained, but they do not account for the effects of dissolution or bioturbation. Sedimentary core tops integrate effects associated with both occurrence and preservation, and are thus better analogs for the conditions typical of the geological record, but uncertainties in seasonal preferences and the depth of calcification can in some cases lead to misleading inference of secondary environmental sensitivities (Hönisch et al., 2013; Hertzberg & Schmidt, 2013).

Here, we use both core top and laboratory culture data to develop a suite of Bayesian hierarchical models for Mg/Ca. We collate over 1,000 sedimentary Mg/Ca measurements to formulate new calibrations for four major planktic groups: *Globigerinoides ruber* (including both pink and white chromotypes), *Trilobatus sacculifer*, *Globigerina bulloides*, and *Neogloboquadrina pachyderma* (including *N. incompta*). First, we assess the impact of adding known secondary environmental predictors (bottom water saturation state, salinity, pH and laboratory cleaning technique) to a Mg/Ca calibration model. We then compute both pooled (all species groups considered together) and hierarchical (species groups considered separately) calibration models using Bayesian methodology similar to that previously developed for core top models of planktic foraminiferal $\delta^{18}\text{O}$ (Malevich et al., 2019). We assess the validity of the new regressions by applying them to sediment trap data and downcore measurements of foraminiferal Mg/Ca. Given that planktic foraminiferal Mg/Ca is increasingly used for SST estimation in deeper geological time, we develop a version of our model that accounts for secular changes in the Mg/Ca composition of seawater. The overarching goal of this study is to develop a flexible set of forward and inverse models for planktic foraminiferal Mg/Ca that estimate observational uncertainties and can be used in a variety of paleoclimatic applications, including inter-proxy comparisons, proxy-model comparisons, and data assimilation.

2 Data compilation

We compiled 1279 core-top Mg/Ca measurements from the literature (Rosenthal & Boyle, 1993; Russell et al., 1994; Brown & Elderfield, 1996; Hastings et al., 1998; Mashiotto et al., 1999; Elderfield & Ganssen, 2000; Ganssen & Kroon, 2000; Dekens et al., 2002; Lea et al., 2003; Palmer & Pearson, 2003; Pahnke et al., 2003; Rosenthal et al., 2003; Visser et al., 2003; Schmidt et al., 2004; Barker et al., 2005; Farmer et al., 2005; Keigwin et al., 2005; Oppo & Sun, 2005; Steinke et al., 2005; Sun et al., 2005; Weldeab et al., 2005; Benway et al., 2006; Dahl & Oppo, 2006; Lea et al., 2006; Meland et al., 2006; Regenberg et al., 2006; Weldeab et al., 2006; de Garidel-Thoron et al., 2007; Leduc et al., 2007; Levi et al., 2007; Richey et al., 2007; Stott et al., 2007; Wei et al., 2007; Weldeab et al., 2007; Cléroux et al., 2008; Ferguson et al., 2008; Nürnberg et al., 2008; Steinke et al., 2008; Yu et al., 2008; Kozdon et al., 2009; Mathien-Blard & Bassinot, 2009; Regenberg et al., 2009; Richey et al., 2009; Oppo et al., 2009; Kubota et al., 2010; Linsley et al., 2010; Marchitto et al., 2010; Mohtadi et al., 2010; Xu et al., 2010; Johnstone et al., 2011; Mohtadi et al., 2011; Sabbatini et al., 2011; Thornalley et al., 2011; van Raden et al., 2011; Boussetta et al., 2012; Fallet et al., 2012; Schmidt, Weinlein, et al., 2012; Schmidt, Chang, et al., 2012; J. A. Arbuszewski et al., 2013; Riethdorf et al., 2013; Saraswat et al., 2013; Aagaard-Sørensen et al., 2014; Dyez et al., 2014; Gibbons et al., 2014; Moffa-Sánchez et al., 2014; Romahn et al., 2014; Weldeab et al., 2014; Khider et al., 2015; Rustic et al., 2015; Gebregiorgis et al., 2016; Parker et al., 2016; Tierney et al., 2016; Vázquez Riveiros et al., 2016; Hollstein et al., 2017; Kristjánssdóttir et al., 2017; Morley et al., 2017; Dai et al., 2019). The data collection includes the core name, the site location (latitude, longitude, water depth), the interval of the core sampled (if provided), the Mg/Ca ratio, corresponding $\delta^{18}\text{O}$ and $\delta^{13}\text{C}$ measurements (if provided), the species, the size fraction

113 sampled (if provided) and the source reference. Since previous work points to a system-
 114 atic offset in Mg/Ca based on the cleaning method used in the laboratory (Rosenthal
 115 et al., 2004; Khider et al., 2015), we flagged the data according to the type of cleaning
 116 performed, with a value of 0 assigned to samples cleaned without a reductive step (e.g.,
 117 Barker et al., 2003) and a value of 1 assigned to samples cleaned with the reductive step
 118 (e.g., Boyle & Keigwin, 1985). We assigned a quality control flag to each core top – in-
 119 dicating whether the data should be included in our calibration model or not – based
 120 on the interpretation of the data in the original study. For example, data that were noted
 121 as suspect due to small sample size or encrustation of high-Mg coatings were excluded.
 122 We also excluded data from the eastern Mediterranean, where authigenic high-Mg coat-
 123 ings are commonly observed and result in anomalous Mg/Ca values (Sabbatini et al., 2011).
 124 This initial quality screen reduced our dataset to 1182 samples, with 452 core tops for
 125 *G. ruber* white, 74 for *G. ruber* pink, 292 for *T. sacculifer*, 72 for *N. pachyderma*, 158
 126 for *N. incompta*, and 134 for *G. bulloides* (Fig. 1). *G. ruber* white and pink core top sam-
 127 ples were subsequently combined and averaged and collectively treated as the *G. ruber*
 128 group, recognizing that these chromotypes are closely related genetically (Aurahs et al.,
 129 2011) and have similar geochemistry (Richey et al., 2019, 2012). In addition, initial ex-
 130 ploration indicated that the *G. ruber* pink dataset spanned a limited geographical (tropical-
 131 subtropical Atlantic) and temperature (25–28°C) range, complicating accurate determi-
 132 nation of regression coefficients. Likewise, *N. pachyderma* and *N. incompta* were com-
 133 bined and calibrated together as the *N. pachyderma* group. Originally considered to be
 134 morphotypes, *N. pachyderma* and *N. incompta* are now classified as genetically differ-
 135 ent species (Darling et al., 2006) and have different temperature optima (which is ac-
 136 counted for in our seasonal calibration). However, they have similar habitat preferences,
 137 living seasonally in the high latitudes in the mixed layer (Darling et al., 2006), and as
 138 with *G. ruber* pink, we found that the limited number of *N. pachyderma* core tops chal-
 139 lenged calibration in isolation.

140 The core top data are matched to the nearest gridpoint from the World Ocean At-
 141 las 2013 (WOA13) version 2 (Boyer et al., 2013), from which we draw mean annual and
 142 seasonal SSTs and sea-surface salinity (SSS). As with our previous calibration models
 143 for foraminiferal $\delta^{18}\text{O}$ (Malevich et al., 2019), we do not explicitly consider depth habi-
 144 tat for the different planktic groups. Although regressing against environmental param-
 145 eters at 0 m water depth might not be optimal to derive the ‘true’ sensitivities of Mg/Ca,
 146 we assume that users want to infer past SSTs from mixed-layer species, rather than a
 147 calcification depth temperature. In addition, depth preferences tend to co-vary with sea-
 148 sonal preferences and so accounting for both can lead to overfitting. We tested this as-
 149 sumption by running our Bayesian calibration models using integrated 0–50m values; we
 150 obtained nearly identical coefficients (not shown). We note that any prescribed depth
 151 habitat in a calibration – whether it be 0 m or 0–50m – assumes that it is static in time.
 152 Circumventing this assumption requires modeling depth habitat explicitly as a function
 153 of thermal tolerance, light, and nutrients (e.g., Lombard et al., 2011). This adds consid-
 154 erable complexity, and paleoclimate applications would require biogeochemical constraints,
 155 thus we leave this for future work.

156 Seasonal averages are computed using spatially-varying estimates of when the peak
 157 abundance of each foraminiferal species occurs, according to their individual thermal tol-
 158 erances. As described in Malevich et al. (2019), these are based on kernel density esti-
 159 mates (KDE) of sediment trap data (Žarić et al., 2005) and the seasonal cycle in tem-
 160 perature at each site, as inferred from WOA13. For example, the KDE of *G. ruber* abun-
 161 dance indicates that this species prefers SSTs between 22.5 and 31.9 °C. Thus, for lo-
 162 cations with SSTs that seasonally drop below 22.5°C, *G. ruber* is assumed to not cal-
 163 cify during those months, and the average seasonal SST would be the mean value for all
 164 months above 22.5°C. Effectively, this assumes that *G. ruber* Mg/Ca reflects mean an-
 165 nual SSTs at most tropical locations, but warm-season SSTs in the subtropics. We also
 166 draw seasonal optima for *N. pachyderma* and *N. incompta* separately, recognizing the

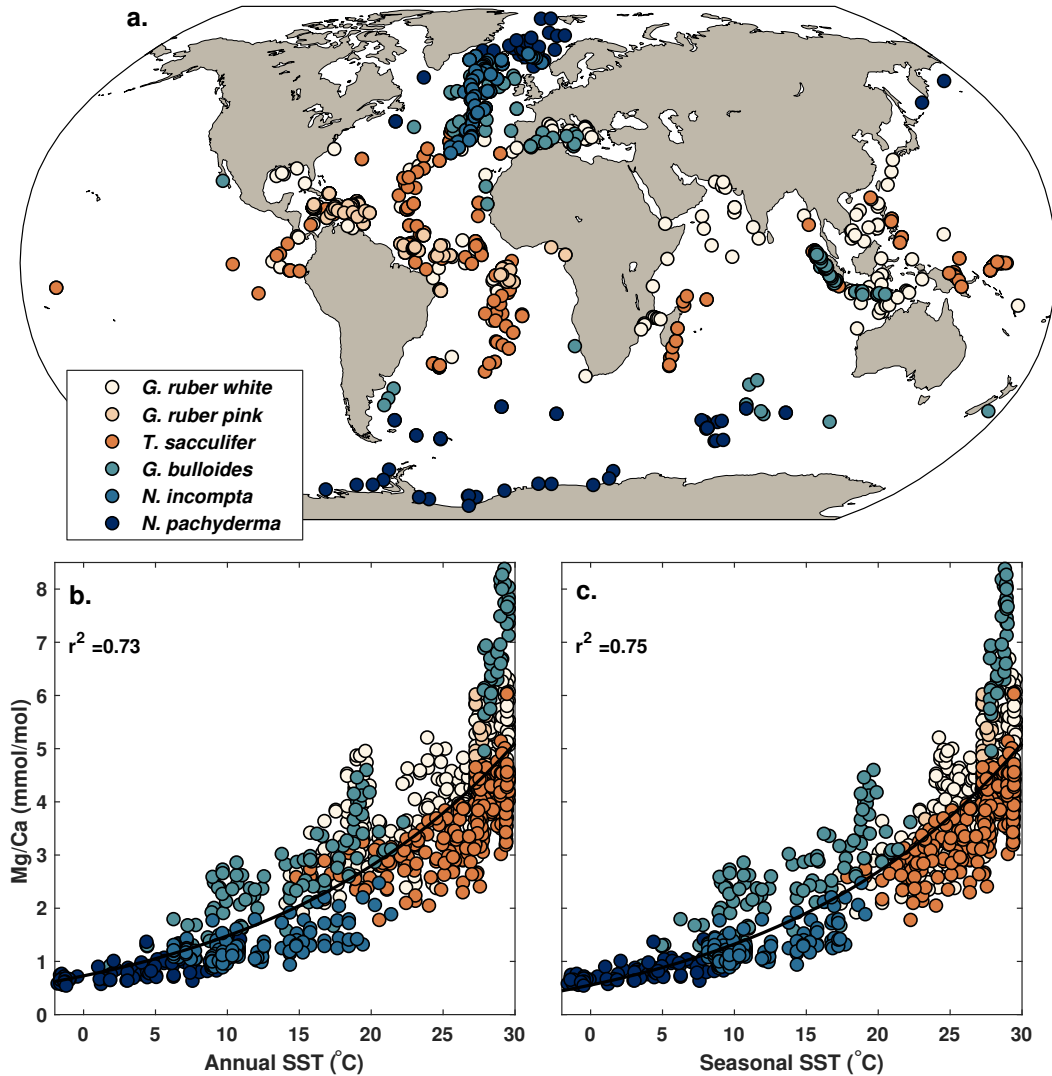


Figure 1. a. Geographical distribution of the Mg/Ca core top data, with an “include” flag of 1 ($N = 1182$), by species. b. The relationship between Mg/Ca and mean annual SSTs. c. The relationship between Mg/Ca and estimated seasonal SSTs. Black lines through the data in (b.) and (c.) represent the best-fit exponential regressions, with r^2 values listed in the upper left.

167 distinct temperature preferences of these two species, even though they are ultimately
 168 calibrated together. Table 1 lists the minimum, maximum, and median SST preferences
 169 for each species according to the KDE method. For *G. ruber*, *T. sacculifer*, and *N. in-*
 170 *compta*, our inferred optimal SST ranges are very similar to those modeled by Lombard
 171 et al. (2009) from culture data (21–30°C; 19–31°C; 6–20°C; respectively). Our ranges
 172 for *G. bulloides* and *N. pachyderma* are slightly larger (Table 1) than the Lombard et
 173 al. (2009) estimates (10–25°C; 0–10°C; respectively) because the sediment trap data in-
 174 dicate a wider thermal range for these species.

175 Core tops that fall within the same gridpoint, and contain the same species, are
 176 further averaged prior to calibration exercises to reduce the impact of spatial clustering
 177 on the regression parameters. This results in an effective core top N of 710 for our re-

Table 1. Sea-surface temperature ranges associated with peak abundances for each foraminiferal species investigated in this study, based on kernel density estimates of shell fluxes from a collection of global sediment traps (from Malevich et al., 2019)

Species	Peak Abundance SST ranges ($^{\circ}\text{C}$)		
	Min	Max	Median
<i>G. ruber</i>	22.5	31.9	27.4
<i>T. sacculifer</i>	20.2	30.6	27.0
<i>G. bulloides</i>	3.6	29.2	18.0
<i>N. pachyderma</i>	-0.9	15.3	5.4
<i>N. incompta</i>	6.7	21.1	15.3

178 gression models, with $N = 307$ for *G. ruber*, $N = 184$ for *T. sacculifer*, $N = 100$ for
179 *G. bulloides* model, and $N = 119$ for *N. pachyderma*.

180 Since previous work indicates that the carbonate system influences foraminiferal
181 Mg/Ca, we also collate surface water pH and bottom water calcite saturation state (Ω)
182 values for each core site from the Global Ocean Data Analysis Project (GLODAP) ver-
183 sion 2 gridded climatology (Lauvset et al., 2016). GLODAPv2 lacks coverage in the Gulf
184 of Mexico, so for core tops in this location we rely on bottle data collected as part of the
185 second Gulf of Mexico and East Coast Carbon Cruise (GOMECC-2) in 2012 (data pub-
186 licly available from <http://www.aoml.noaa.gov/ocd/gcc/GOMECC2>) and use the MAT-
187 LAB implementation of CO2SYS (v1.1, Van Heuven et al., 2011) to compute pH and
188 calcite Ω from measured values of alkalinity, dissolved inorganic carbon, salinity, tem-
189 perature, pressure, silicate, and phosphate. We used the Mehrbach K1 and K2 constants,
190 as refit by A. Dickson and Millero (1987).

191 Overall, our core top dataset spans a wide range of SSTs (-1.8 to 29.6°C ; 95% CI
192 = 3.1 to 29.4°C) and Ω (0.7 to 5.5 ; 95% CI = 0.9 to 3.3). Although high and low SSS
193 values are represented in the dataset (28.4 to 38.6 psu), the distribution of the data is
194 more restricted (95% CI = 33.3 to 37.5 psu). The range of surface water pH values sam-
195 pled is limited (7.97 to 8.22 ; 95% CI = 8.02 – 8.17), reflecting the fact that the pH of the
196 modern surface ocean does not have a large dynamic range.

197 As described below, we also use Mg/Ca data from cultured foraminifera to con-
198 strain sensitivities to environmental parameters. We use the compilation of Gray and
199 Evans (2019), with the addition of the *G. ruber* pink data from Allen et al. (2016) and
200 *N. incompta* data from Von Langen et al. (2005) and Davis et al. (2017). This updated
201 culture dataset includes 30 *G. ruber* observations, 20 *T. sacculifer* observations, 12 *G.*
202 *bulloides* observations, 29 *O. universa* observations and 12 *N. incompta* observations for
203 a total of 103 data points.

204 **3 Model form and exploration of environmental predictors**

205 Temperature clearly exerts a strong, non-linear control on core top Mg/Ca, explain-
206 ing about 75% of the variance in the data (Fig. 1b,c), in agreement with experimental
207 evidence (e.g., Lea et al., 1999). However, laboratory studies and previous core top in-
208 vestigations have shown that pH, salinity, the saturation state (Ω) at the core site, the
209 cleaning method, and shell size also influence Mg/Ca. Mg/Ca sensitivities to salinity and
210 pH are also considered exponential (Lea et al., 1999; Kisakürek et al., 2008; Hönisch et
211 al., 2013; Evans, Wade, et al., 2016; Gray et al., 2018). Culture experiments suggest a
212 pH sensitivity of -50 to -90% per pH units for *O. universa*, *G. bulloides*, and *G. ruber*
213 (white) (Lea et al., 1999; Russell et al., 2004; Kisakürek et al., 2008; Evans, Brierley, et

214 al., 2016; Gray & Evans, 2019), and Gray et al. (2018) detected a pH sensitivity of a sim-
 215 ilar magnitude of $-80\% \pm 70\%$ (2σ) per pH units in a global compilation of *G. ruber* (white)
 216 sediment trap data. However, pH does not seem to impact Mg/Ca in cultures of *N. pachy-*
 217 *derma*, *N. incompta* (Davis et al., 2017) and *T. sacculifer* (Allen et al., 2016). Labora-
 218 tory experiments indicate a moderate sensitivity of planktic Mg/Ca to salinity (3–5%
 219 per psu) (Lea et al., 1999; Kisakürek et al., 2008; Hönisch et al., 2013; Allen et al., 2016;
 220 Gray & Evans, 2019). Previous core top studies suggested a much larger sensitivity (15–
 221 59%, Ferguson et al., 2008; Mathien-Blard & Bassinot, 2009; J. Arbuszewski et al., 2010)
 222 but reanalyses indicated that these high estimates are due either to environmental co-
 223 variates (Hertzberg & Schmidt, 2013; Hönisch et al., 2013; Khider et al., 2015) or an-
 224 alytical issues (Dai et al., 2019). Core top observations also reveal a systematic decline
 225 in sedimentary planktic Mg/Ca – regardless of species – under low bottom water Ω at
 226 the site of deposition (Regenberg et al., 2014). Finally, intra- and inter-laboratory com-
 227 parisons (Barker et al., 2003; Rosenthal et al., 2004) as well as a regression analysis of
 228 *G. ruber* (white) core tops (Khider et al., 2015) indicate a systematic offset in measured
 229 Mg/Ca of ~ 10 – 15% based on whether the laboratory cleaning method includes a reduc-
 230 tive step. Mg/Ca also varies by shell size (Elderfield et al., 2002; Friedrich et al., 2012),
 231 but researchers tend to mitigate this effect by picking foraminifera from a restricted size
 232 fraction. Preliminary investigations revealed that shell size was not a significant predic-
 233 tor for core top Mg/Ca, so it is not included in our models.

234 Since temperature, salinity, and pH sensitivities are exponential, we transform Mg/Ca
 235 to $\ln(\text{Mg/Ca})$ for model fitting. This transformation also assumes that the errors for a
 236 Mg/Ca model follow an exponential distribution; the data in Figure 1b and 1c suggest
 237 that this is a valid assumption, as variance increases non-linearly with temperature. Fol-
 238 lowing Khider et al. (2015), the cleaning parameter acts as a multiplicative term in Mg/Ca
 239 space, and thus an additive term in $\ln(\text{Mg/Ca})$ space, with the understanding that reduc-
 240 tive cleaning (a value of 1) results in a systematic decline in Mg/Ca. The form of the
 241 Mg/Ca dependency on Ω is less clear. Regenberg et al. (2014) and Khider et al. (2015)
 242 assume that bottom water saturation impacts Mg/Ca of tests linearly below a certain
 243 threshold, which they define based on ΔCO_3^{2-} instead of Ω . These two quantities are
 244 functionally equivalent, but we prefer using Ω because it is always a positive value. How-
 245 ever, it might be expected, based on reaction kinetics, that Mg/Ca should have a non-
 246 linear dependency on saturation state, with dissolution increasing as saturation state drops
 247 (Sjöberg, 1976). Indeed, if we remove the impact of SST on our pooled dataset, we find
 248 that $\ln(\text{Mg/Ca})$ residuals trend non-linearly with Ω , with the slope becoming steeper as
 249 Ω becomes smaller (Fig. 2). The relationship is strongest below an Ω of ~ 1.5 (Fig. 2),
 250 which is consistent with the ΔCO_3^{2-} threshold of $\sim 40 \mu\text{mol/kg}$ identified by Regenberg
 251 et al. (2014). Ω sensitivity can be approximated by a power function, with a coefficient
 252 of -2 (Fig. 2). This supports a transformation of Ω to Ω^{-2} in order to linearize the sen-
 253 sitivity of $\ln(\text{Mg/Ca})$ to saturation state.

254 The final form of a core top Mg/Ca forward model, based on the physical expecta-
 255 tions outlined above, is:

$$256 \quad \ln(\text{Mg/Ca}) = \alpha + \mathbf{T} \cdot \beta_T + \mathbf{S} \cdot \beta_S + \mathbf{pH} \cdot \beta_P + \mathbf{\Omega}^{-2} \cdot \beta_O + (1 - \mathbf{clean} \cdot \beta_C) + \epsilon, \quad (1)$$

$$257 \quad \epsilon \sim \mathcal{N}(\mathbf{0}, \sigma^2)$$

258 where ϵ is the vector of residual errors, approximated by a Normal distribution with mean
 259 zero and variance σ^2 .

260 To assess the impact of each environmental variable on model performance, we it-
 261 eratively computed regressions using ordinary least squares, adding each predictor se-
 262 quentially. We then compared the Bayesian Information Criterion (BIC) for each iter-
 263 ative model to determine whether the additional predictor resulted in improvement. The
 264 BIC is a criterion for model selection that helps guard against overfitting by penalizing

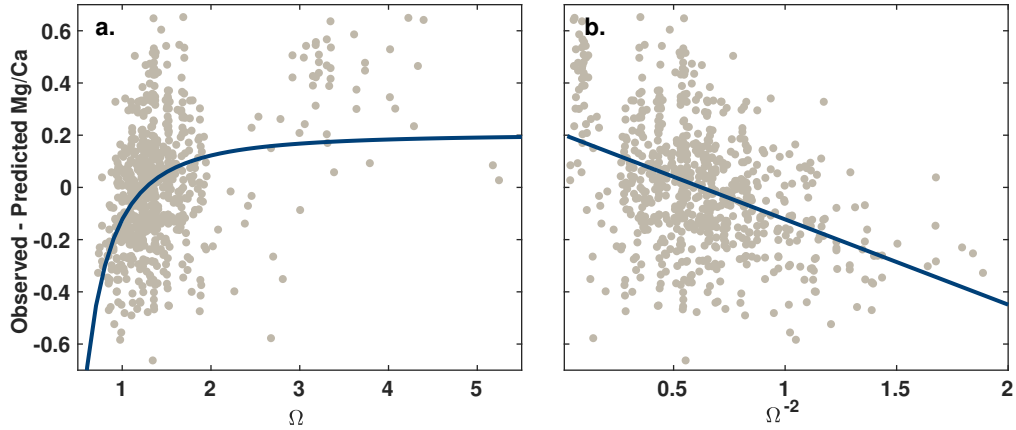


Figure 2. The relationship of core top $\ln(\text{Mg}/\text{Ca})$ residuals (observed-predicted; all species; $N = 710$) to a. bottom water calcite Ω and b. Ω^{-2} after removing the dependence on temperature. Dots represent individual core tops; lines show the best fit regression.

265 the addition of parameters that don't improve the model fit; lower values (regardless of
 266 sign) indicate a better fit. We also analyzed the significance of each predictor's coeffi-
 267 cient. We do this for both the pooled dataset (using annual and seasonal SST and SSS
 268 estimates) and the four species groups (using seasonal SST and SSS estimates), and dis-
 269 cuss the results for each predictor in turn.

270 3.1 Temperature

271 For both the pooled annual and pooled seasonal datasets, we find that SST alone
 272 explains over 80% of the variance in $\ln(\text{Mg}/\text{Ca})$ (Table 2). This is slightly greater than
 273 an exponential model for Mg/Ca (Fig. 1b and c), reflecting some improvement in the
 274 fit associated with the assumption that variance increases exponentially. Temperature
 275 remains the most important parameter for the individual species models, although, it
 276 explains only ca. 50% of the variance for the warm-water groups (*G. ruber* and *T. sac-*
 277 *culifer*; Table 2). This is due to the relatively restricted temperature ranges for *G. ru-*
 278 *ber* and *T. sacculifer* (ca. 12°C) compared to those for *G. bulloides* and *N. pachyderma*
 279 (> 20°C), which allows for more variance to be explained by the other environmental
 280 factors. The temperature sensitivity is similar across all species, between 5–7% (Table
 281 2). This agrees well with recent re-assessments from culture and sediment traps, both
 282 of which indicate a temperature sensitivity of ca. 6% (Gray et al., 2018; Gray & Evans,
 283 2019) rather than 9%, as previously assumed (e.g., Dekens et al., 2002; Anand et al., 2003;
 284 Khider et al., 2015).

285 3.2 Bottom water calcite saturation (Ω)

286 The addition of Ω as a predictor improves almost all of the models (r^2 increases,
 287 RMSE decreases, and BIC decreases), with the biggest impact on the warm-water species
 288 (Table 2). The large drop in BIC associated with the addition of this parameter (to the
 289 pooled models in particular, where it is about 100) supports long-standing theory and
 290 intuition that inclusion of Ω improves prediction of core top Mg/Ca (Rosenthal & Boyle,
 291 1993; Russell et al., 1994; Brown & Elderfield, 1996; Rosenthal et al., 2000; Dekens et
 292 al., 2002; Regenberg et al., 2014). Ω sensitivity remains fairly constant across species groups,
 293 in agreement with previous work that most species of planktic foraminifera are sensitive
 294 to saturation state at the site of deposition (Regenberg et al., 2014). The possible ex-

295 ception is the *N. pachyderma* group, for which Ω is not a significant predictor (Table 2).
 296 Ω ranges between 0.75 and 2.8 within this group, hence the lack of sensitivity does not
 297 reflect a limitation of the data. It may be that *N. pachyderma* and *N. incompta*, which
 298 have a thicker outer calcite crust than the other species considered here, are indeed less
 299 sensitive to dissolution, in agreement with buoy exposure experiments (Berger, 1970),
 although the error on the Ω coefficient is large (± 0.1 , 2σ).

Table 2. Regression model metrics and coefficients. RMSE = root mean square error (in $\ln(\text{Mg}/\text{Ca})$ units). Each column notes the addition (or subtraction) of a predictor relative to the column to the left. Group-specific models were calculated with seasonal temperature and salinity estimates. BIC = Bayesian Information Criterion. Lower values indicate improved performance. n denotes the number of core tops (after gridding, see Section 2). Coefficients correspond to that of the added predictor. Coefficients in italics are not significantly different than zero (at $p = 0.05$).

	SST	+ Ω^{-2}	+ clean	+ SSS	-SSS +pH
<i>Pooled annual, n = 710</i>					
r^2	0.83	0.86	0.87	0.87	0.87
RMSE	0.24	0.22	0.21	0.21	0.21
BIC	2	-135	-198	-210	-193
Coefficient	0.063	-0.35	0.16	0.029	<i>0.30</i>
<i>Pooled seasonal, n = 710</i>					
r^2	0.85	0.87	0.89	0.89	0.89
RMSE	0.22	0.21	0.19	0.19	0.19
BIC	-114	-210	-293	-288	-289
Coefficient	0.064	-0.27	0.17	<i>-0.004</i>	<i>0.36</i>
<i>G. ruber n = 307</i>					
r^2	0.55	0.66	0.71	0.71	0.71
RMSE	0.15	0.13	0.12	0.12	0.12
BIC	-284	-363	-407	-403	-404
Coefficient	0.068	-0.24	0.11	<i>0.002</i>	<i>0.28</i>
<i>T. sacculifer, n = 184</i>					
r^2	0.51	0.68	0.73	0.73	0.77
RMSE	0.13	0.11	0.10	0.10	0.09
BIC	-214	-287	-318	-314	-339
Coefficient	0.055	-0.27	0.12	<i>0.006</i>	1.4
<i>G. bulloides, n = 100</i>					
r^2	0.86	0.88	0.88	0.89	0.89
RMSE	0.19	0.17	0.17	0.17	0.17
BIC	-44	-60	-57	-54	-55
Coefficient	0.068	-0.29	<i>0.12</i>	<i>-0.024</i>	<i>-1.0</i>
<i>N. pachyderma, n = 119</i>					
r^2	0.78	0.79	0.80	0.80	0.80
RMSE	0.15	0.15	0.15	0.15	0.15
BIC	-109	-107	-108	-106	-106
Coefficient	0.052	<i>-0.06</i>	0.088	<i>0.047</i>	<i>0.57</i>

3.3 Cleaning

The addition of the cleaning parameter (0 for samples without the reductive step, 1 for samples with the reductive step) improves the statistics for the pooled models and the warm-water groups, with drops in BIC on the order of 10–50 (Table 2) but has little impact on *G. bulloides* and *N. pachyderma*. In the case of *G. bulloides*, this reflects a limitation of the data subset: all but two of the core tops were cleaned with the oxidative protocol, so it is not possible to reliably detect the influence of reductive cleaning. For *N. pachyderma*, the influence of cleaning on model skill is small but the derived coefficient (9%) is close to the other species (11–12%), and is in agreement with previous estimates (Barker et al., 2003; Rosenthal et al., 2004; Khider et al., 2015). Overall, the change in BIC suggests that inclusion of laboratory cleaning does notably improve prediction of core top Mg/Ca and, the limitation of the *G. bulloides* data subset aside, the sensitivity should be relatively consistent across species, as expected from laboratory investigations (Barker et al., 2003).

3.4 Salinity

The addition of salinity to the model does not significantly improve the statistics for the species group regressions, nor for the pooled seasonal model (BIC is mostly unchanged; Table 2). The inferred sensitivity to salinity is low or statistically insignificant in all of these cases. There is moderate improvement in the pooled annual model (BIC drops by 12) and the inferred sensitivity is higher (2.9% per psu), consistent with the best estimate from culture studies ($3.6 \pm 1.2\%$, 2σ ; Gray & Evans, 2019). Overall, these results suggest that the addition of salinity neither improves nor degrades core top Mg/Ca prediction, and furthermore that the derived salinity sensitivity from the core top dataset is essentially negligible. This result is not due to our choice to calibrate to surface salinity; derived sensitivities from 0–50 m average values yield equally low values (not shown). Rather, the accuracy of the derived salinity sensitivities is restricted by both the limited range of values in our core top dataset (95% CI = 33.3 to 37.5 psu), and the strong covariation between temperature and salinity that is typical of global ocean. Since the high latitudes are fresh and cold, and the subtropics warm and salty, below SSTs of 21°C, SST and SSS are positively correlated in our dataset ($\rho = 0.87$, $p < 0.0001$). Since the tropics are warm and fresh, above 21°C SST and SSS are negatively correlated ($\rho = -0.73$, $p < 0.0001$). Even though the direction of the correlation flips, this high degree of relation creates a condition of collinearity, especially for the group data subsets as they fall on one side of the relationship or the other. This means that the OLS-derived coefficients for SSS are not reliable.

3.5 pH

The addition of pH degrades model performance and/or yields insignificant or unrealistic coefficients (Table 2). The expected sensitivity from laboratory experiments is $-70 \pm 14\%$ per pH unit; in comparison, our coefficients are generally of the incorrect sign (Table 2). This is unsurprising given the restricted range of values (8.02–8.17, 95% CI) in our dataset, and more broadly, in the modern ocean. In addition, pH is collinear with temperature ($r = -0.70$, $p < 0.0001$), because cold locations have a higher pH. It is also possible that the water column pH observations derived from the GLODAPv2 product are inaccurate. Point GLODAP measurements from the upper water column may not fully sample seasonal and year-to-year variability, and include the impact of anthropogenic CO₂, which, in most locations, would not be represented in core top Mg/Ca values. Overall, our regression analysis demonstrates that Mg/Ca sensitivity to pH cannot be reliably recovered from core top data.

3.6 Summary of environmental sensitivities

Our iterative regression analysis identifies temperature, Ω , and the laboratory cleaning method as significant predictors of core top Mg/Ca. Salinity and pH sensitivities cannot be accurately determined from the core top dataset due to collinearity, a limited range of values, and possible inaccuracies in observations. From an empirical point of view, these findings support the omission of salinity and pH from the Mg/Ca model. However, it is well-known from culture studies that salinity and pH are important influences on Mg/Ca, and can bias estimates of past temperatures (Khider et al., 2015; Gray & Evans, 2019). We therefore retain these predictors, but in order to provide better constraints on their coefficients, we develop Bayesian hierarchical models in which both the culture and core top data are used to constrain parameters. This model structure leverages the information in both the experimental (laboratory) data and the empirical (core top) data, ultimately allowing for more accurate prediction of Mg/Ca.

4 BAYMAG: Bayesian calibration models for Mg/Ca

4.1 Model design

Following our previous work with $\delta^{18}\text{O}$ of foraminifera (Malevich et al., 2019), we developed two styles of forward models to represent core top Mg/Ca: one that pools all species together (mainly for deep-time applications with extinct species) and another that treats each species group separately, with information shared through parameters and hyperparameters. The pooled model design is:

$$\ln(\text{Mg/Ca}_c) = \begin{cases} \alpha_i + \mathbf{T}_c \cdot \beta_{Tc} + \mathbf{S}_c \cdot \beta_S + \epsilon_c & \text{if } \textit{incompta}, \textit{sacculifer} \\ \alpha_i + \mathbf{T}_c \cdot \beta_{Tc} + \mathbf{S}_c \cdot \beta_S + \mathbf{pH}_c \cdot \beta_P + \epsilon_c & \text{if } \textit{ruber}, \textit{bulloides}, \textit{universa} \end{cases} \quad (2)$$

$$\epsilon_c \sim \mathcal{N}(\mathbf{0}, \sigma_{ci}^2)$$

$$\ln(\text{Mg/Ca}) = \alpha + \mathbf{T} \cdot \beta_T + \mathbf{S} \cdot \beta_S + \mathbf{pH} \cdot \beta_P + \Omega^{-2} \cdot \beta_O + (1 - \textit{clean}) \cdot \beta_C + \epsilon, \quad (3)$$

$$\epsilon \sim \mathcal{N}(\mathbf{0}, \sigma^2)$$

with different values of α and σ for each i cultured species. Hyperparameters on the culture temperature coefficient are:

$$\beta_{Tc} \sim \mathcal{N}(\mu_{\beta T}, \sigma_{\beta T}^2) \quad (4)$$

and the culture temperature coefficient acts as a prior on the core top temperature coefficient:

$$\beta_T \sim \mathcal{N}(\beta_{Tc}, \sigma_{\beta T}^2) \quad (5)$$

The top of the model hierarchy (Eq. 2) describes Mg/Ca in the culture dataset (see Section 2 for a description of the data compilation) and accounts for the fact that Mg/Ca in cultures of *N. incompta* and *T. sacculifer* is not sensitive to pH (Allen et al., 2016; Davis et al., 2017). Otherwise, the temperature, salinity, and pH sensitivities are assumed to be similar across cultured species, while the intercept and error terms are allowed to vary between each species i to account for offsets in the mean and variance of $\ln(\text{Mg/Ca})$. As a reality check, we run this top part of the model independently to assess how well it predicts culture Mg/Ca data alone. We find that this top hierarchy yields excellent prediction and the posterior coefficients for temperature, salinity, and pH are similar to previous assessments done with an ordinary least squares approach (Gray & Evans, 2019) (Fig. 3), validating our model design.

The lower part of the hierarchy (Eq. 3) contains the model for the core top data. Since the core tops are pooled together across all species, it assumes a generic pH sensitivity. The pH and salinity sensitivities (β_P and β_S) are constrained by the culture data

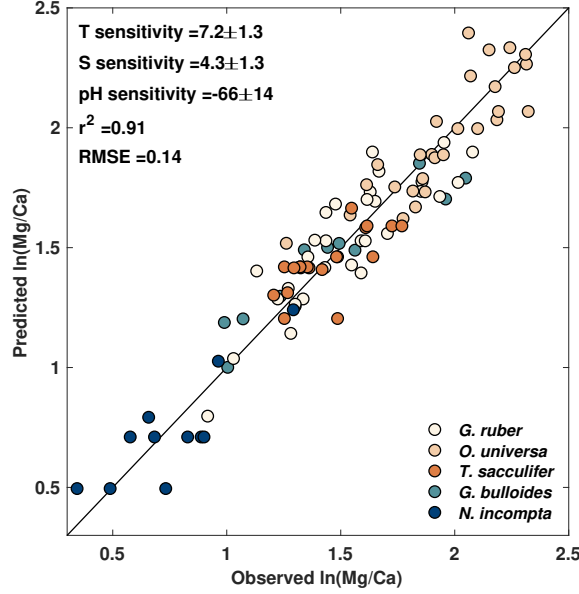


Figure 3. Bayesian hierarchical model results for planktic Mg/Ca culture data, including median and 2σ ranges for the posterior temperature, salinity, and pH sensitivities.

390 in the top part of the hierarchy, and then allowed to influence the core top data. Con-
 391 versely, the sensitivities to Ω and the cleaning method (β_O and β_C) are only constrained
 392 by the core top data. The temperature sensitivities β_{T_c} and β_T are constrained by both
 393 the culture and core top data, with the former acting as the prior mean for the latter.

394 The group-specific core top model takes the slightly modified form,

$$\ln(\text{Mg}/\text{Ca}_c) = \begin{cases} \alpha_i + \mathbf{T}_c \cdot \beta_{T_c} + \mathbf{S}_c \cdot \beta_S + \epsilon_c & \text{if } \textit{incompta}, \textit{sacculifer} \\ \alpha_i + \mathbf{T}_c \cdot \beta_{T_c} + \mathbf{S}_c \cdot \beta_S + \mathbf{pH}_c \cdot \beta_P + \epsilon_c & \text{if } \textit{ruber}, \textit{bulloides}, \textit{universa} \end{cases} \quad (6)$$

$$\epsilon_c \sim \mathcal{N}(\mathbf{0}, \sigma_{ci}^2)$$

395

$$\ln(\text{Mg}/\text{Ca}) = \begin{cases} \alpha_j + \mathbf{T} \cdot \beta_T + \mathbf{S} \cdot \beta_S + \Omega^{-2} \cdot \beta_O + (1 - \textit{clean} \cdot \beta_C) + \epsilon & \text{if } \textit{pachy}, \textit{sacculifer} \\ \alpha_j + \mathbf{T} \cdot \beta_T + \mathbf{S} \cdot \beta_S + \mathbf{pH} \cdot \beta_P + \Omega^{-2} \cdot \beta_O + (1 - \textit{clean} \cdot \beta_C) + \epsilon & \text{if } \textit{ruber}, \textit{bulloides} \end{cases} \quad (7)$$

$$\epsilon \sim \mathcal{N}(\mathbf{0}, \sigma_i^2)$$

396 with hyperparameters and priors on the temperature coefficients as above (Eqs. 4 and
 397 5). The top part of the hierarchy (Eq. 6), describing the culture data, is identical to the
 398 pooled model (Eq. 2). The lower part of the hierarchy (Eq. 7) describes the core top data,
 399 and since species are treated independently, accounts for the fact that the *T. sacculifer*
 400 and *N. pachyderma* core tops should not be sensitive to pH. As with the culture data,
 401 the intercept and error terms (α_j and σ_j) are allowed to vary for each j foraminiferal
 402 species. The temperature, salinity, Ω and cleaning sensitivities are computed across all
 403 of the data and are not allowed to vary by species. This choice was made because our
 404 regression experiments indicated that, with few exceptions, these sensitivities are sim-
 405 ilar across species (Table 2). Although we did observe a lower Ω sensitivity for the *N.*
 406 *pachyderma* group (see Section 3.2), computation of a hierarchical model with group-
 407 specific Ω coefficients yielded no improvement in model skill. Likewise, computation of
 408 group-specific temperature coefficients did not improve skill, supporting our assumption

409 (and inferences from the culture data) that temperature sensitivity should be similar across
410 species.

411 For all models, we estimate parameters using Bayesian inference and Markov chain
412 Monte Carlo sampling (Gelman et al., 2003) with Stan software, version 2.19.1 (Carpenter
413 et al., 2017). Prior distributions for the parameters and hyperparameters, as well as prior
414 vs. posterior plots, are given in Appendix A. To assess the impact of using annual vs.
415 seasonal SST and SSS, we computed the pooled and group-specific models with both sets
416 of values, although we recommend use of either the pooled annual or group-specific sea-
417 sonal models for practical applications. We perform Pareto-Smoothed Importance Sam-
418 pling Leave-One-Out (psis-loo) cross-validation to compare predictive accuracy between
419 models (Vehtari et al., 2017). These values are reported as expected log pointwise pre-
420 dictive density (elpd); larger values indicate a better fit to the data.

421 4.2 Model results

422 The pooled annual model explains 87% of the variance in the core top Mg/Ca data
423 and has a median root mean square error (RMSE) of 0.21 ln(Mg/Ca) units (Fig. 4a).
424 Analysis of the Mg/Ca residuals yields no significant trends with the SST, SSS, Ω , and
425 cleaning predictors. There is a weak correlation between the residuals and core top pH
426 (Spearman’s $\rho = 0.15$, $p < 0.0001$) but as discussed above, we are unsure whether the
427 core top pH observations are accurate. Likewise, the posterior coefficients for the pH pre-
428 dictor are very similar to the those derived from the culture data alone (Fig. 3) reflect-
429 ing limited influence from the core top data. The derived salinity sensitivity is also close
430 to culture expectations at 3.8%. The median temperature coefficient is lower than the
431 culture value (6.4 vs. 7.2) although by design, is still the same within uncertainty. This
432 shift reflects the influence of the core top data, which act to narrow the temperature sen-
433 sitivity down to a precise estimate of 6.4 ± 0.2 (2σ).

434 While as a whole the residuals are well-distributed across the zero line, there are
435 systematic offsets according to species (Fig. 4b). This is expected, as neither seasonal-
436 ity nor species differences are accounted for in the pooled model. Generally speaking,
437 the model over-predicts Mg/Ca for *N. pachyderma* and *T. sacculifer* (Fig. 4d and f) and
438 under-predicts Mg/Ca for *G. ruber* and *G. bulloides* (Fig. 4c and e). These species-level
439 offsets likely reflect differences in depth habitat. *N. pachyderma* is typically interpreted
440 to inhabit the upper 100 m of the water column (Reynolds & Thunell, 1986; Elderfield
441 & Ganssen, 2000; Mortyn & Charles, 2003; Taylor et al., 2018), which would integrate
442 cooler temperatures than SST and lead to lower observed ln(Mg/Ca). This may explain
443 model overestimation in the high-latitudes (Fig. 4f). Likewise, in the tropics *T. sacculifer*
444 is often found in a slightly deeper habitat than *G. ruber* (Erez & Honjo, 1981; Fairbanks
445 et al., 1980; Ravelo & Fairbanks, 1992), leading to lower Mg/Ca than predicted from sur-
446 face temperatures. This expected offset between *G. ruber* and *T. sacculifer* can be seen
447 visually in Fig. 4a; at higher values of ln(Mg/Ca), *T. sacculifer* plots to the left of *G.*
448 *ruber*. This explains model over-estimation in the tropics (Fig. 4d). The pooled model
449 underestimates *G. bulloides* Mg/Ca nearly everywhere, because this species tends to have
450 higher average Mg/Ca values than *N. pachyderma*, *G. ruber*, and *T. sacculifer* (Elderfield
451 & Ganssen, 2000; Cl eroux et al., 2008) (Fig. 4e).

452 It is not surprising then that model performance improves markedly with the use
453 of seasonal SST and SSS and group-specific parameters. The most significant improve-
454 ment comes from accounting for differences between foraminiferal groups (Eq. 7), which
455 cause elpd, a measure of predictive accuracy, to rise from 100–150 to 400–450, indicat-
456 ing a much improved fit (Fig. 5). The seasonal, group-specific model can account for 95%
457 of the variance in the core top data (Fig. 6) with an RMSE comparable to that of the
458 culture regression (Fig. 3). As with the pooled model, there is no significant correlation
459 between the cleaning and Ω predictors and the residuals and a weak positive correlation

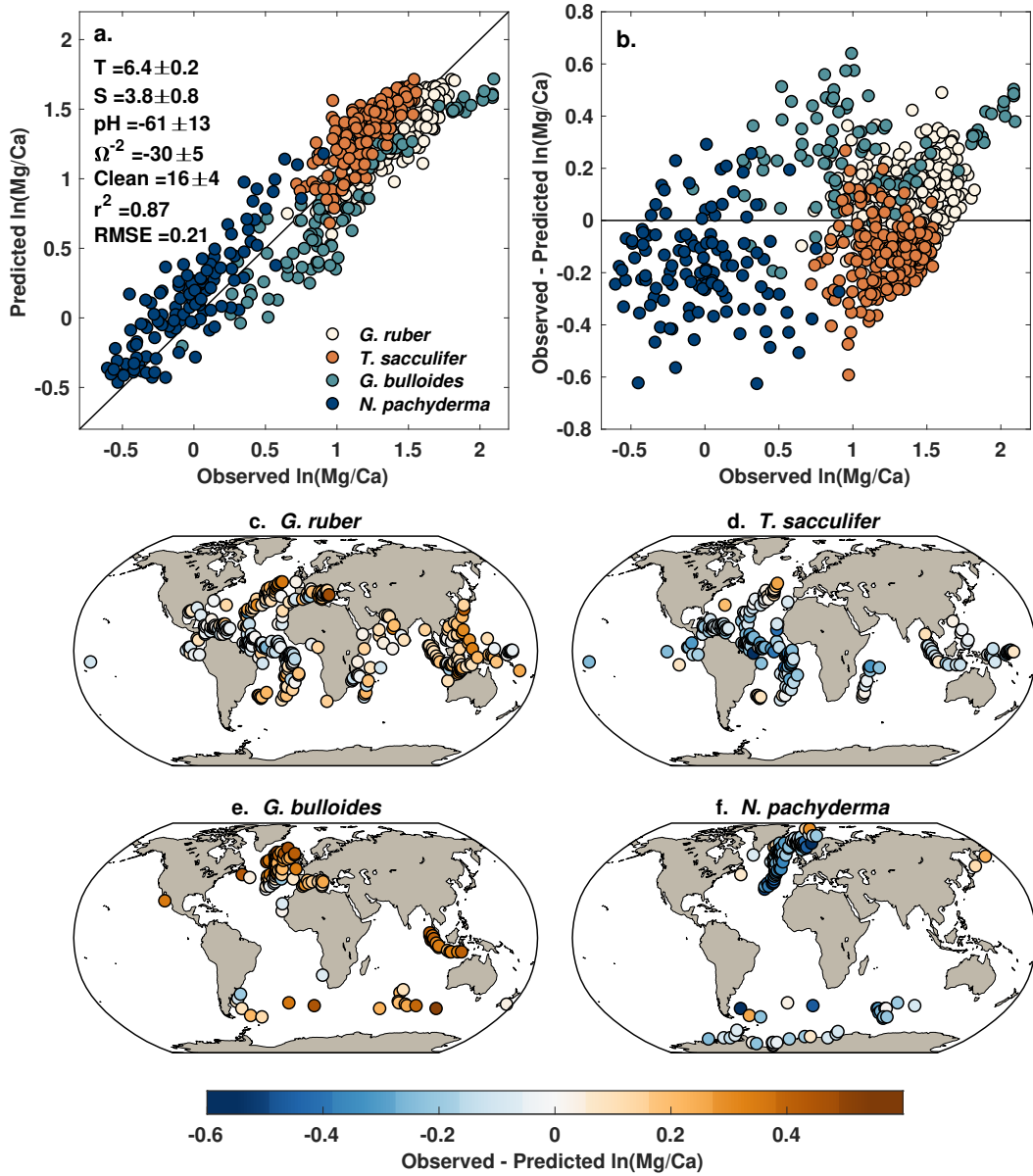


Figure 4. Pooled annual model results. a. Observed vs. predicted $\ln(\text{Mg}/\text{Ca})$, including posterior coefficients for each environmental predictor, colored by species group; b. Model residuals, colored by species group; c.-f. Maps of model residuals for each species group.

460 with the pH predictor ($\rho = 0.11, p = 0.003$). There are however weak correlations between
 461 the residuals and both temperature and salinity ($\rho = 0.13, p = 0.0008$; $\rho = -0.21,$
 462 $p < 0.0001$). The negative correlation with salinity is seen in all species groups except
 463 *T. sacculifer* and represents the model balance between the strong salinity sensitivity
 464 inferred from the culture data (4.3%, Fig. 3) and the weak salinity sensitivity that is re-
 465 covered from the core top data when seasonal SSTs are used (Table 2). As discussed in
 466 Section 3.4, the core top-derived salinity sensitivities are affected by collinearity between
 467 SST and SSS, and therefore may not be accurate. To enforce a sensitivity that is consis-
 468 tent with the culture data, we applied an informative prior to the salinity parameter
 469 (see Appendix). The posterior salinity coefficient is still significantly smaller than that

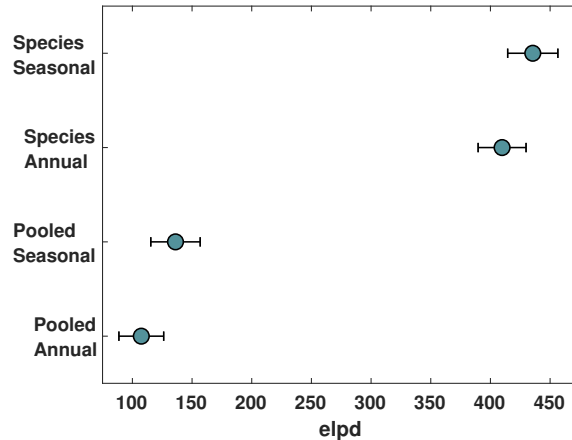


Figure 5. Expected log pointwise predictive density (elpd), based on psis-loo cross validation, for each Bayesian model. Higher values indicate better fit.

470 of the pooled model (1.7 ± 0.7 vs. 3.8 ± 0.8) due to core top influence, but is higher than
 471 it otherwise would be without this constraint.

472 The correlation between residuals and temperature seems to be mostly driven by
 473 *G. ruber* residuals, which also show a strong trend with observed $\ln(\text{Mg}/\text{Ca})$ ($r = 0.70, p <$
 474 0.0001). This could indicate that temperature sensitivity for *G. ruber* is systematically
 475 underestimated; however, the trend is only slightly ameliorated after running a version
 476 of the group-specific model with variable SST coefficients for each species ($r = 0.61, p <$
 477 0.0001), and the derived ca. 6% sensitivity of the seasonal group-specific model is very
 478 similar to values calculated from *G. ruber* culture and sediment trap data (Gray et al.,
 479 2018; Gray & Evans, 2019). Alternatively, this residual trend could suggest that our relatively
 480 simple inference of seasonal SST (based on sediment trap abundances) doesn't
 481 apply well to *G. ruber*. However, we did not see this residual trend in our model for $\delta^{18}\text{O}$
 482 of *G. ruber*, which uses the same seasonal estimation method (Malevich et al., 2019). Ac-
 483 counting for subtle differences in depth habitat would make the trend worse, as studies
 484 suggest that *G. ruber* should have a deeper habitat in the tropics (and therefore lower
 485 Mg/Ca) and shallower one in the subtropics (and therefore higher Mg/Ca) (Hertzberg
 486 & Schmidt, 2013; Hönisch et al., 2013). Similar to *G. ruber*, a group of *G. bulloides* data
 487 with very high Mg/Ca also falls to the right of the one-to-one line (Fig. 6). These data
 488 are from the Sumatran margin, where *G. bulloides* calcifies primarily during the cooler
 489 upwelling season, at a depth of ca. 50 m (Mohtadi et al., 2009). This preference should
 490 cause negative, rather than the observed positive, residuals. Taken together, the *G. bul-*
 491 *loides* and *G. ruber* residuals suggest that Mg/Ca sensitivity to temperature may, in fact,
 492 be more non-linear than our model (and all previous exponential models) have assumed,
 493 or alternatively that there is a latent environmental variable or vital effect that scales
 494 non-linearly with temperature. This latent effect is most prominent in *G. ruber* and ac-
 495 counts for the fact that our model can only explain 67% of the variance in *G. ruber* Mg/Ca.
 496 In contrast, our model can explain 73%, 88%, and 77% of the variance in Mg/Ca for *T.*
 497 *sacculifer*, *G. bulloides*, and *N. pachyderma*, respectively.

498 Further investigation is needed to properly diagnose what this latent variable might
 499 be, but the fact that impacts *G. ruber* and *G. bulloides* preferentially suggests that it
 500 could be pH. pH scales inversely with temperature; warm locations have lower pH and
 501 would be associated with higher Mg/Ca than expected from temperature alone. Although
 502 pH is included in our model, if the GLODAP measurements are inaccurate then this ef-
 503 fect would not be fully accounted for in our Mg/Ca predictions and produce the kind

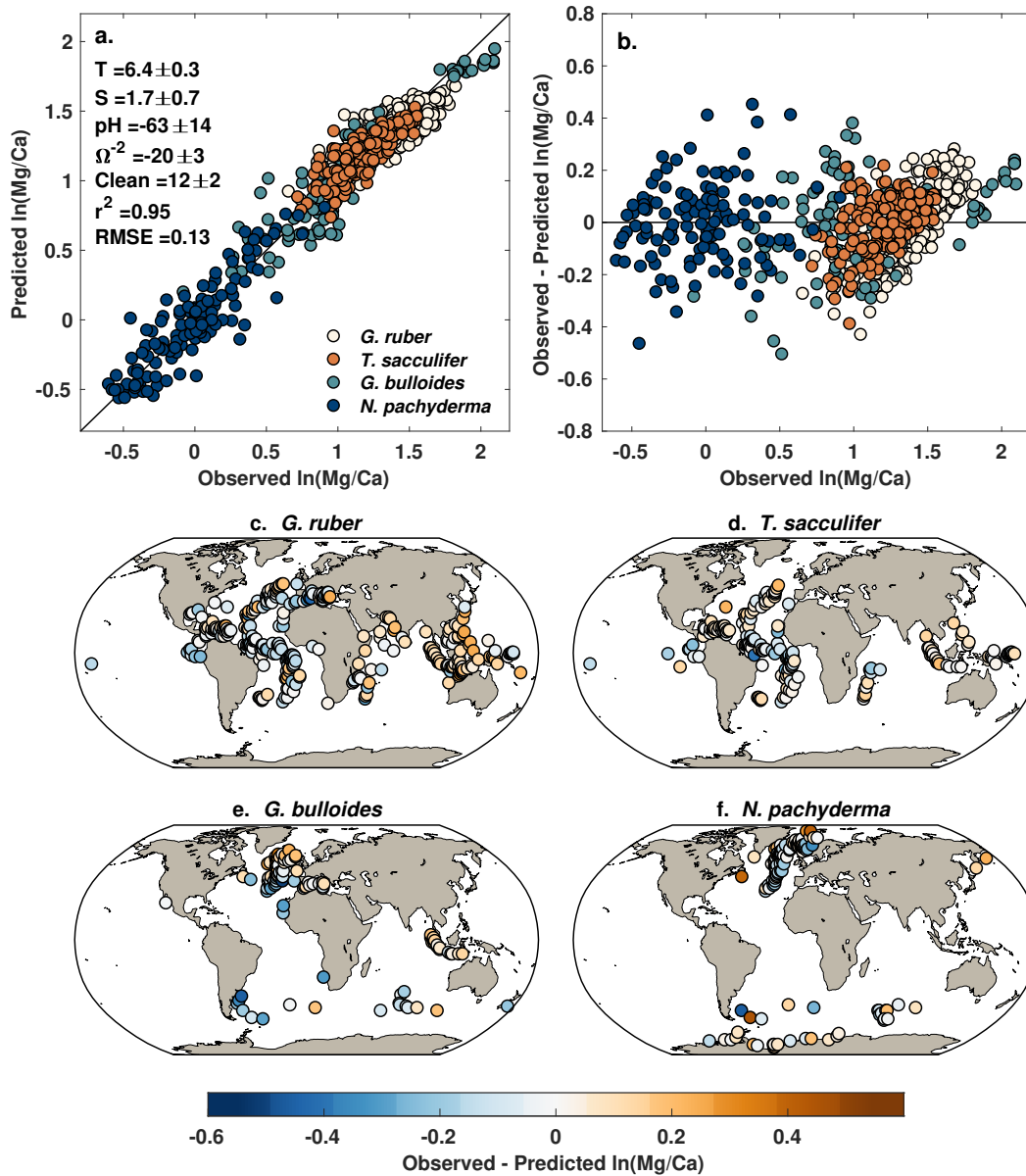


Figure 6. Seasonal, group-specific model results. a. Observed vs. predicted ln(Mg/Ca), including posterior coefficients for each environmental predictor, colored by species group; b. Model residuals, colored by species group; c.-f. Maps of model residuals for each species group.

504 of residual trends we observe. Indeed, tropical regions, such as the eastern equatorial Pa-
 505 cific and Indo-Pacific warm pool, are poorly observed in the GLODAP dataset, and these
 506 are also locations where the residual error is notably low and high, respectively, for *G.*
 507 *ruber* (Fig. 6c).

508 In spite of the residual trends, the magnitude of the residual bias is still very small
 509 (0.13 ln(Mg/Ca) units, 1σ), and out-of-sample applications of BAYMAG in Section 5
 510 suggest that our model yields good prediction of *G. ruber* Mg/Ca.

511 The seasonal group-specific model eliminates the species-level offsets seen in the
 512 pooled annual model by allowing the intercept terms to vary for each foraminiferal group

(Fig. 6b). These intercept terms effectively compensate for depth habitat preference as well as any offsets in average Mg/Ca incorporation. Many of the strong spatial trends in residuals are also minimized (Fig. 6c–f) when compared to the pooled model (Fig. 4c–f), although some patterns remain. In addition to patterns that may reflect the impact of the latent variable discussed above, there are negative residuals for *G. bulloides* in the west African and Benguela upwelling zones; along frontal regions in the Southern Ocean; and near the confluence of the Brazil and Malvinas currents (Fig. 6e) indicating that Mg/Ca values are lower than the model predicts. Similar patterns were observed in the residuals of our Bayesian $\delta^{18}\text{O}$ models (Malevich et al., 2019) and might suggest that *G. bulloides* is calcifying during either a cooler season than our seasonal SST inferences predict, or in a deeper habitat. These patterns could also conceivably reflect geochemical differences between *G. bulloides* genotypes (Sadekov et al., 2016) or high productivity driving locally-enhanced dissolution (Hertzberg & Schmidt, 2013).

5 Application of the BAYMAG forward model

Forward modeling of Mg/Ca is useful for model-data comparison, and data assimilation techniques that rely on forward models to translate model output into proxy units (Hakim et al., 2016). BAYMAG can be used to model new values of Mg/Ca (\tilde{y}) from observed or simulated SST, SSS, pH, Ω , and cleaning protocol by simply drawing from the posterior predictive distribution, $\tilde{y} \sim \mathcal{N}(\mu, \sigma^2)$, where μ and σ are the core top component of either the pooled annual or group-specific seasonal model (Eqs. 3, 7). If the user desires, a prior can be used to restrict values to reasonable outcomes; e.g., for *G. ruber*, Mg/Ca values over 6.5 are rarely observed in the modern ocean (0% of core tops, 1% of sediment traps). To provide an example, as well as to test our model on out-of-sample data, we apply BAYMAG to monthly average observations of SST, SSS, and pH at two locations that have multi-year foraminiferal Mg/Ca sediment trap data (Fig. 7). For the Gulf of Mexico site, we used the SST, SSS, and pH climatologies (adjusted values) provided in the source publication (Richey et al., 2019). For the Gulf of California site, we used average monthly SSTs reported in the source publication (McConnell & Thunell, 2005), WOA13 climatology for SSS, and pH climatology as estimated by Gray et al. (2018). Ω is set to 5.7 for the Gulf of Mexico and 3.4 for the Gulf of California; since these values are high, they have minimal impact on predicted Mg/Ca. Both studies used a non-reductive cleaning protocol, so the cleaning value is set to 0. In all cases we use the group-specific, seasonal model; although temperatures and salinity vary month-by-month in this case, we assume that the seasonal model most accurately captures the ‘true’ environmental sensitivities. Weak priors on Mg/Ca were used to assign a low probability (< 5%) to Mg/Ca values above 7 and 9 for *G. ruber* and *G. bulloides*, respectively (Fig. 7).

Overall, the BAYMAG predictions match observed Mg/Ca values well, almost always overlapping within the 1σ range (Fig. 7). This is an encouraging result, because our model is calibrated on core top foraminifera that have been affected by dissolution and sedimentary processes, while the sediment trap data consist of more pristine specimens. BAYMAG slightly overestimates *G. ruber* Mg/Ca in the Gulf of Mexico (Fig. 7a), even though our model residuals suggest that it should under-predict high values (Fig. 6b), suggesting that the residual trends have a minimal impact on prediction.

6 Inversion of BAYMAG to predict past SST

Since BAYMAG is a multivariate model, inversion to predict past SSTs requires constraints on salinity, pH, and Ω . In the simplest case, these can be held constant at modern values, but this assumes that only temperature caused observed variation in Mg/Ca. More realistic inference can be derived from making informed assumptions about past changes. For example, over the Quaternary glacial cycles, it is reasonable to assume that

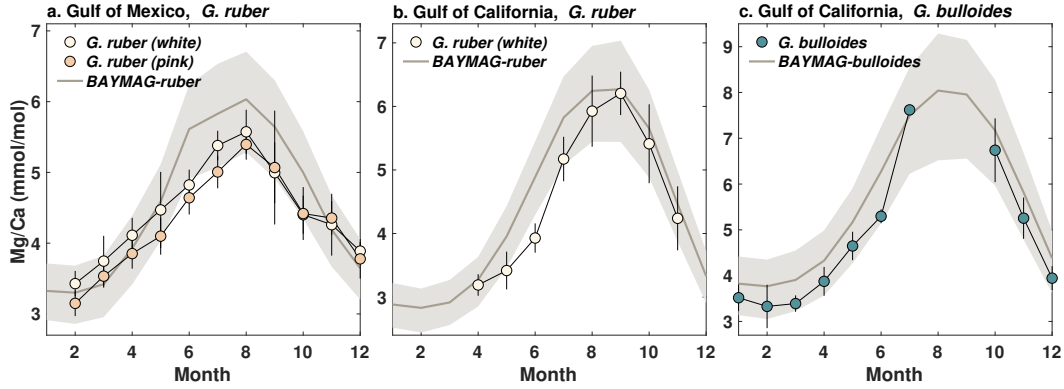


Figure 7. Forward-modeled Mg/Ca from BAYMAG, compared to sediment trap observations from the Gulf of Mexico (Richey et al., 2019) and Gulf of California (McConnell & Thunell, 2005). Normal priors of $\mathcal{N} \sim (4, 1.5)$ and $\mathcal{N} \sim (5, 2)$ were used for *G. ruber* and *G. bulloides*, respectively. The Gulf of Mexico data were shifted backwards by 1 month to account for sinking and integration time. No adjustments to the Gulf of California data were made; this is a shallower trap (485 m vs. 1150 m) and the data indicate minimal lag. Shading and error bars represent 1σ uncertainties.

563 surface water pH and salinity both increased during glacial periods due to lower atmo-
 564 spheric CO_2 and lower sea level. It is also possible to leverage information from inde-
 565 pendent proxies sensitive to changes in the oceanic carbonate system, such as $\delta^{11}\text{B}$ (for
 566 surface pH) or benthic B/Ca (for Ω). Alternatively, output from a climate or biogeochem-
 567 ical model could be used to provide constraints.

568 To facilitate SST prediction for diverse applications, we provide two versions of the
 569 Bayesian inverse model for Mg/Ca. One assumes that salinity, pH, and Ω are known,
 570 allowing for quick computation of posterior SST. The other treats all of the environmen-
 571 tal predictors as unknowns, and allows the user to place prior distributions on them. This
 572 latter model involves joint computation of posterior temperature, salinity, pH, and Ω and
 573 is therefore slower to converge, but has the advantage of propagating uncertainty in these
 574 co-variates into the estimation of SST.

575 To demonstrate use of the inverse models, we apply BAYMAG to three sites that
 576 have Late Quaternary Mg/Ca data as well as independent estimates of SST from alkenone
 577 $\text{U}_{37}^{K'}$ (Fig. 8a). In each case, we use the appropriate seasonal, group-specific model; how-
 578 ever, our KDE method for inferring seasonality predicts that foraminifera at all three
 579 of these locations should reflect mean annual temperature. We draw modern Ω and sur-
 580 face pH value for each site from GLODAPv2 (Lauvset et al., 2016), and modern salin-
 581 ity from WOA13 (Boyer et al., 2013). In all cases, we use a prior standard deviation of
 582 6°C , and assume that pH, salinity, and Ω are error-free; we found that including errors
 583 on these factors only slightly increases error bars (not shown).

584 For the Holocene data at site MD99-2269 in the North Atlantic, we assume that
 585 salinity, and Ω are constant through time (*N. pachyderma* is not sensitive to pH). We
 586 find that BAYMAG predicts latest Holocene SST values that are in good agreement with
 587 modern observed annual SST, whereas the calibration (Elderfield & Ganssen, 2000) used
 588 in the original publication (Kristjánsson et al., 2017) slightly underestimates SSTs (Fig.
 589 8b). The BAYMAG predictions suggest that annual SSTs have declined through the Holocene
 590 by about 3°C . In contrast, the $\text{U}_{37}^{K'}$ data from this site show a weaker long-term trend,
 591 and are also much warmer than the *N. pachyderma* predictions (Fig. 8b). $\text{U}_{37}^{K'}$ at this

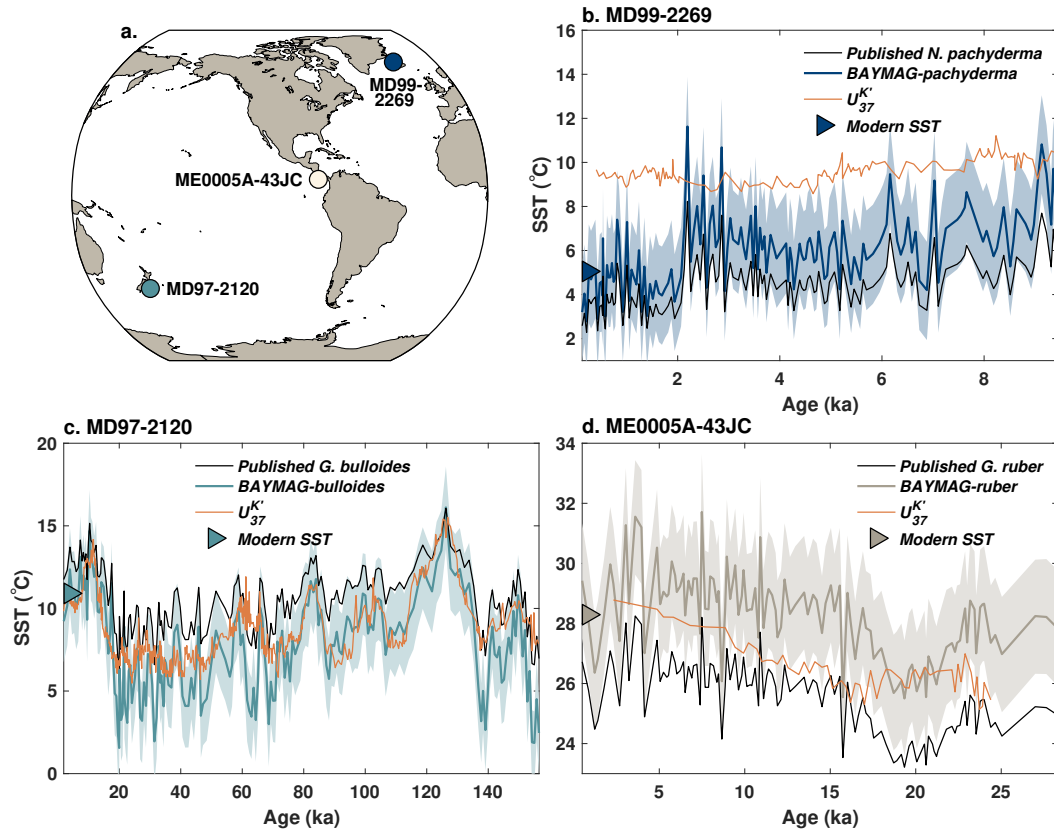


Figure 8. Example applications of BAYMAG to predict past SSTs. a) Locations of targeted Late Quaternary sites b) *N. pachyderma* data from MD99-2269 (66.6°N, 20.9°W, 365 m, Kristjánsdóttir et al., 2017) c) *G. bulloides* data from MD97-2120 (45.5°S, 174.9°E, 1210 m, Pahnke et al., 2003) d) *G. ruber* data from ME0005A-43JC (7.9°N, 83.6°W, 1368 m, Benway et al., 2006). At each location, data are compared to $U_{37}^{K'}$ SST estimates (median values, calibrated with BAYSPLINE, Tierney & Tingley, 2018). Triangles show modern mean annual SSTs at each site. Shading indicates 1σ uncertainties.

592 latitude (66°N) is assumed to reflect late summer temperatures (August–October) (Tierney
 593 & Tingley, 2018); however modern August–October SSTs at this site (6.4°C) are still
 594 much cooler than the latest Holocene $U_{37}^{K'}$ values (ca. 9.5°C, Fig. 8b). This might indicate
 595 that $U_{37}^{K'}$ production is restricted to only the warmest of summer months; alternatively the
 596 warm bias could reflect the influence of sea ice. This site sits close to the boundary where
 597 substantial seasonal sea ice is present in the modern day, and anomalously high $U_{37}^{K'}$
 598 values occur in areas of extensive sea ice cover (Filippova et al., 2016; Tierney & Tingley,
 599 2018).

600 For site MD97-2120 in the South Pacific, we make some rudimentary assumptions
 601 of how pH and salinity may have varied over glacial-interglacial cycles. Following Gray
 602 et al. (2018) and Gray and Evans (2019), we assume that global pH increased by 0.13
 603 units during the Last Glacial Maximum due to lowered CO_2 . We then scaled the normalized
 604 ice core CO_2 curve (Bereiter et al., 2015) to this value and added it to the modern
 605 site estimate of pH to simulate past changes. For this site, this results in a range of
 606 pH values between 8.12 (modern value) to 8.25 (maximum glacial value). For salinity,
 607 we scaled the normalized sea level curve to an inferred LGM change of 1.1 psu and added
 608 this to the site estimate, for a range between 34.4 (modern values) to 35.5 (maximum

glacial value). We then interpolate these scaled curves to the ages at which there are Mg/Ca observations, and input them into BAYMAG. We do not explicitly account for the temperature effect on pH (e.g., Gray & Evans, 2019) because while it scales with the magnitude of local cooling, it is a small source of error for the LGM (0.65°C, Gray & Evans, 2019). Since the salinity and pH sensitivities are of opposite sign, the glacial-interglacial changes partly cancel each other out; however, LGM cooling is still 0.8°C warmer than estimates made with constant salinity and pH (not shown) due to the pH effect.

The BAYMAG predictions from *G. bulloides* Mg/Ca at MD97-2120 produce latest Holocene SSTs in good agreement with modern mean annual values, and yield cooler median values and a larger glacial-interglacial range than the calibration (Mashiotta et al., 1999) used in the original publication (Pahnke et al., 2003) (Fig. 8c). There is generally a good match with alkenone $U_{37}^{K'}$, except during the coldest times of the glacial periods (Fig. 8c). The cold predictions in part reflect the fact that the glacial *G. bulloides* Mg/Ca values at this site are at the limit of the modern calibration dataset, and the group-specific model has a tendency to over-predict Mg/Ca (and thus under-predict SSTs) at southern latitudes (Fig. 6e). A tighter prior could mitigate this effect; however, this example illustrates that caution should be exercised when extrapolating BAYMAG to values of Mg/Ca that are near the edge or outside of the calibration range.

Finally, we tested BAYMAG on *G. ruber* data from site ME0005A-43JC, in the eastern Pacific warm pool. We scale salinity and pH estimates in the same manner as at site MD97-2120. Varying salinity and pH results in glacial estimates that are ca. 0.9°C warmer than a constant assumption (not shown). Latest Holocene BAYMAG predictions once again align well with modern SSTs, and are overall warmer than the published estimates (Benway et al., 2006), which used the Anand et al. (2003) calibration without a correction for dissolution (Fig. 8d). Although this site is not particularly deep, it sits in a relatively corrosive location – modern Ω is 0.95 – thus BAYMAG assumes some Mg/Ca loss from dissolution. The magnitude of glacial cooling agrees well with the $U_{37}^{K'}$ estimates, although the two proxies have different trajectories through the deglaciation and the Holocene (Fig. 8d). The different trajectories could reflect differences in the seasonal production of alkenones and *G. ruber* (Timmermann et al., 2014); however, core top studies in the eastern equatorial Pacific do not find any evidence for a seasonal bias in alkenone signatures (Kienast et al., 2012; Tierney & Tingley, 2018).

7 Use of BAYMAG on longer geological timescales

7.1 Incorporating changes in Mg/Ca of seawater

When Mg/Ca is used to infer SSTs on million-year timescales, data must be corrected for secular changes in the Mg/Ca ratio of seawater (Mg/Ca_{sw}). Ancient Mg/Ca_{sw} values can be independently estimated from fossil corals (Gothmann et al., 2015), halite fluid inclusions (Lowenstein et al., 2001; Horita et al., 2002; Brennan et al., 2013), calcium carbonate veins (Coggon et al., 2010), echinoderm ossicles (J. Dickson, 2002, 2004), and paired Mg/Ca-clumped isotope measurements of benthic foraminifera (Evans et al., 2018). Although some of these Mg/Ca_{sw} estimates have large uncertainties, and are also sometimes poorly dated, they clearly indicate a non-linear increase in Mg/Ca_{sw} over the past 200 Ma, with the most rapid change occurring in the last 30 Ma (Fig. 9a). The reason for the increase is still not certain; magnesium isotope evidence and geochemical modeling suggests that it could reflect a decrease in Mg incorporation into marine clays (Higgins & Schrag, 2015; Dunlea et al., 2017).

To develop a version of BAYMAG that accounts for changing Mg/Ca_{sw} , we created a 1,000-member ensemble of possible Mg/Ca_{sw} trajectories by Monte Carlo sampling the uncertainties in both age assignment and Mg/Ca_{sw} of each estimate in Figure 9a, interpolating to a 0.5 Ma timestep, and applying a 13 Ma (the residence time of

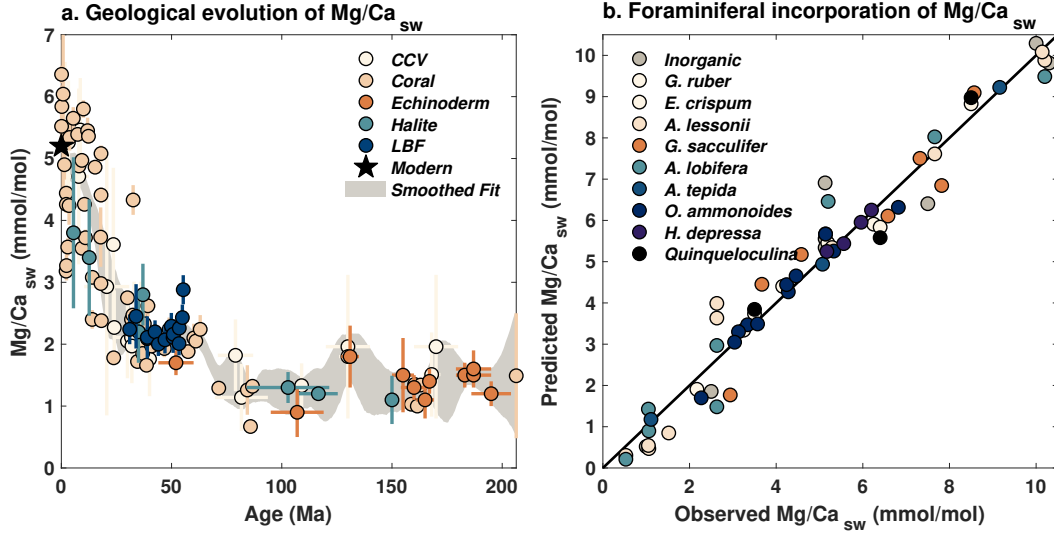


Figure 9. a. Evolution of Mg/Ca_{sw} over the past 200 Ma, according to Mg/Ca measured in calcium carbonate veins (CCV, Coggon et al., 2010), fossil corals (Gothmann et al., 2015), echinoderm ossicles (J. Dickson, 2002, 2004), halite fluid inclusions (Lowenstein et al., 2001; Horita et al., 2002; Brennan et al., 2013), and large benthic foraminifera (LBF, Evans et al., 2018). Star denotes the modern value of 5.2 mmol/mol (Horita et al., 2002). Shading encloses the 95% CI of an ensemble of Gaussian smoothed fits to the data, used in the seawater-enabled BAYMAG models. b. Relationship between observed Mg/Ca_{sw} and linear predictions of Mg/Ca_{sw} from Mg/Ca of calcite in laboratory inorganic precipitation (Mucci & Morse, 1983) and foraminiferal culture studies (Delaney et al., 1985; Segev & Erez, 2006; Raitzsch et al., 2010; Mewes et al., 2014; Evans et al., 2015; Evans, Brierley, et al., 2016; De Nooijer et al., 2017; Hauzer et al., 2018).

659 Mg) Gaussian smooth (Fig. 9a). The resulting collection of curves is then used to cal-
 660 culate Mg/Ca_{sw} for each time t for a given Mg/Ca data series, and then used in the pre-
 661 diction model, i.e.:

$$662 \ln(\mathbf{Mg}/\mathbf{Ca}) = \alpha_j + \mathbf{T} \cdot \beta_T + \mathbf{S} \cdot \beta_S + \mathbf{pH} \cdot \beta_P + \mathbf{\Omega}^{-2} \cdot \beta_O + (1 - \mathbf{clean} \cdot \beta_C) + \frac{\text{Mg}/\text{Ca}_{sw_t}}{\text{Mg}/\text{Ca}_{sw_0}} + \epsilon, \quad (8)$$

$$663 \epsilon \sim \mathcal{N}(\mathbf{0}, \sigma_i^2)$$

664 Previous work has suggested that the incorporation of Mg into calcite varies non-
 665 linearly with Mg/Ca_{sw} , necessitating a power function correction (Evans & Müller, 2012),
 666 rather than a simple ratio between the past value and the modern value as we suggest
 667 above. To re-examine whether such an adjustment is necessary, we compiled experimen-
 668 tal data in which planktic and benthic foraminifera were cultured at varying Mg/Ca_{sw}
 669 concentrations (Delaney et al., 1985; Segev & Erez, 2006; Raitzsch et al., 2010; Mewes
 670 et al., 2014; Evans et al., 2015; Evans, Brierley, et al., 2016; De Nooijer et al., 2017; Hauzer
 671 et al., 2018), along with an inorganic precipitation experiment (Mucci & Morse, 1983)
 672 (Fig. 9b). These data span values of Mg/Ca_{sw} from 0.5 – 10 mmol/mol (Fig. 9b), which
 673 encompasses the range found throughout the Phanerozoic (0.5–6 mmol/mol, J. Dickson,
 674 2002, 2004). For each species (and the inorganic experiment), we computed an ordinary
 675 least squares regression between Mg/Ca_{sw} and Mg/Ca_c , and used the resulting coeffi-
 676 cients to predict Mg/Ca_{sw} from Mg/Ca_c . If there were a non-linear relationship between
 677 Mg/Ca_{sw} and Mg/Ca_c , then the predictions should show curvature away from the the

678 1:1 line. We find that when all the experiments are considered together, this is not the
 679 case – a power function fit to the predictions, of the form $y = a \times x^b$, yields a value of
 680 b close to 1 (0.97 ± 0.07 , 2σ) suggesting no significant curvilinear behavior. Power fits
 681 to predictions from individual species (and the inorganic experiment) also yield values
 682 of b insignificantly different from 1, confirming that the relationship between Mg/Ca_{sw}
 683 and Mg/Ca_c is adequately described by a linear function. The slope of this relationship
 684 varies substantially between species; however, since Mg/Ca_{sw} is ratioed to the modern
 685 value (Eq. 8), this term cancels out. This analysis does not preclude non-linear incor-
 686 poration of Mg into calcite at very low Mg/Ca_{sw} concentrations (<0.5 mmol/mol); how-
 687 ever, such concentrations are not observed in the Phanerozoic. Thus, we conclude that
 688 a power function adjustment is not necessary for paleoclimate applications.

689 More recently, it has been proposed that the temperature sensitivity of Mg/Ca in
 690 foraminifera changes with Mg/Ca_{sw} (Evans, Brierley, et al., 2016). However, thus far this
 691 has only been detected in a culture experiment of *G. ruber*; a study of benthic foraminiferal
 692 species did not detect a change in temperature sensitivity with Mg/Ca_{sw} (De Nooijer
 693 et al., 2017). We therefore do not incorporate this aspect into our model; further exper-
 694 imental evidence supporting this effect is needed.

695 7.2 Applications

696 To test our Mg/Ca_{sw} -enabled models, we apply BAYMAG to representative Ceno-
 697 zoic Mg/Ca data. First, we use the seasonal, group-specific model to predict SSTs from
 698 *T. sacculifer* data from Site ODP 806, in the western Pacific warm pool (Wara et al.,
 699 2005). We assume that salinity and pH are constant through time and error-free, and
 700 use a prior standard deviation of 6°C (Fig. 10a). These data span the early Pliocene (5.3
 701 Ma) to present, over which time Mg/Ca_{sw} has evolved from 4.8 ± 0.2 (2σ) mmol/mol
 702 to the current value of 5.2 mmol/mol, according to our ensemble estimate. Although this
 703 is a small change, it does impact SST prediction, as can be seen from comparison with
 704 the published SST estimates (Wara et al., 2005), which use the Dekens et al. (2002) cal-
 705 ibration and did not account for changing Mg/Ca_{sw} (Fig. 10a). Whereas the original
 706 SST estimates suggest that Pliocene SSTs were consistently cooler than modern, the BAY-
 707 MAG estimates indicate that they were mostly similar to, or warmer than, modern val-
 708 ues and bring the data into better agreement with independent estimates from the TEX₈₆
 709 proxy (Zhang et al., 2014) (Fig. 10a).

710 Next, we apply BAYMAG to Mg/Ca data from the Early Eocene Climatic Opti-
 711 mum (EECO, 53.3–49.1 Ma), one of the warmest times during the Cenozoic Era. These
 712 data include *Morozovella* spp. from site ODP 865 (Tripathi et al., 2003), hemipelagic out-
 713 crops from the eastern shore of New Zealand (mid-Waipara, Tawanui, Tora, and Ham-
 714 pden Beach, C. J. Hollis et al., 2009, 2012; Hines et al., 2017), and DSDP Site 277 (Hines
 715 et al., 2017). *Morozovella* spp. species are extinct, so we do not know their seasonal or
 716 depth habitat preferences. Thus, we use the pooled annual model, which provides generic
 717 constraints on temperature, salinity, pH, and Ω sensitivities. Following Evans et al. (2018),
 718 we assume, based on carbon modeling constraints (Tyrrell & Zeebe, 2004), that ocean
 719 pH is approximately 7.7 during the EECO. Since we have no good knowledge of how salin-
 720 ity changed, we hold it constant at a value of 34.5 for each site. For Ω , we test two as-
 721 sumptions: 1) that the foraminifera are essentially pristine, unaltered by seafloor disso-
 722 lution ($\Omega = 5$), and 2) that the foraminifera have experienced dissolution on par with
 723 what we would expect at the site locations today. For this latter assumption, we draw
 724 Ω from GLODAPv2 using the paleolatitude and paleolongitude (calculated from Baatsen
 725 et al. (2016), as suggested in C. Hollis et al. (2019)) and the inferred Eocene water depth
 726 as described in the original publication. We use an uninformative prior standard devi-
 727 ation of 10°C .

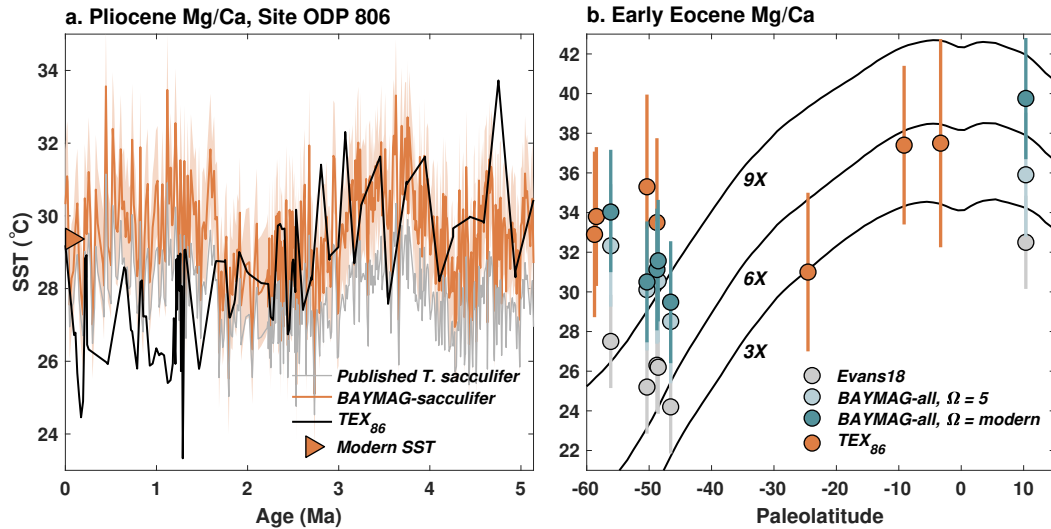


Figure 10. Application of BAYMAG to Cenozoic Mg/Ca data, with correction for changing Mg/Ca_{sw} . a) Mg/Ca data extending back to the Pliocene from Site ODP 806 (Wara et al., 2005). Triangle indicates modern mean annual SST. b) Mg/Ca data (Tripathi et al., 2003; C. J. Hollis et al., 2009, 2012; Hines et al., 2017) from the Early Eocene climatic optimum (53.3–49.1 Ma), plotted by paleolatitude. Black lines denote predicted SSTs from Eocene climate model simulations conducted under 3X, 6X, and 9X preindustrial CO_2 levels (Zhu et al., 2019). In both panels, TEX_{86} data (calibrated with BAYSPAR, Tierney & Tingley, 2014) are plotted for comparison. Shading and error bars represent 1σ uncertainties.

728 We compare our results to the inferences made by Evans et al. (2018) using the same
 729 Mg/Ca data, as well as independent estimates of SST from EECO TEX_{86} data span-
 730 ning similar paleolatitudes (Pearson et al., 2007; Bijl et al., 2009; C. J. Hollis et al., 2009,
 731 2012; Bijl et al., 2013; Inglis et al., 2015; Cramwinckel et al., 2018) calibrated with BAYSPAR
 732 (Tierney & Tingley, 2014; C. Hollis et al., 2019) (Fig. 10b). All of the estimates from
 733 BAYMAG are warmer, on average, than those of Evans et al. (2018), by $4.3^\circ C$ under the
 734 assumption of no dissolution, and by $5.8^\circ C$ with modern Ω estimates (Fig. 10b). Since
 735 our inferred Mg/Ca_{sw} value for the Eocene (2.2 mmol/mol) is the same as Evans et al.
 736 (2018), this difference reflects model form. Evans et al. (2018) first correct Mg/Ca for
 737 the pH effect using laboratory constraints (Evans, Wade, et al., 2016) and then calcu-
 738 late SST assuming a reduced temperature sensitivity at lower Mg/Ca_{sw} , using coefficients
 739 derived from *G. ruber* culture experiments (Evans, Brierley, et al., 2016).

740 In the absence of information concerning the Eocene carbonate system, Evans et
 741 al. (2018) assume no loss from dissolution at depth. For shallow and intermediate-depth
 742 sites considered here, allowing some dissolution increases median SST estimates up by
 743 $0.3\text{--}1.5^\circ C$ – a relatively minor effect. ODP 865 is an exception: here, using a modern
 744 estimate of Ω yields median SST estimates that are $3.9^\circ C$ higher. This is because plate
 745 rotations (Herold et al., 2014; Baatsen et al., 2016) predict that this site was located much
 746 closer to the equator ($4\text{--}10^\circ N$, vs. $18^\circ N$ today) and farther east ($138\text{--}144^\circ W$, vs. $179^\circ W$
 747 today) during the EECO. Today, the eastern equatorial Pacific is very corrosive, even
 748 at intermediate water depths. If EECO Pacific ocean chemistry was similar, then the Mg/Ca
 749 values at ODP 865 would imply very high SSTs (ca. $39^\circ C$, Fig. 10b). This illustrates
 750 how assumptions about Ω can have a large impact on SST estimation from Mg/Ca mea-
 751 sured in pelagic settings, especially over timescales when ocean chemistry may have changed
 752 substantially.

753 BAYMAG SST predictions agree more closely with EECO TEX₈₆ data than the
 754 Evans et al. (2018) calculations (Fig. 10b). Tropical SSTs inferred from Site 865 sup-
 755 port TEX₈₆ inferences of ca. 36°C, and match output from an Eocene climate model sim-
 756 ulation run under 6X preindustrial CO₂ (Zhu et al., 2019). The Mg/Ca predictions sup-
 757 port TEX₈₆ in detecting unusually high SSTs at sites near New Zealand (50–55°S pa-
 758 leolatitude) that are not easily explained by elevated CO₂; these data may reflect changes
 759 in ocean circulation leading to localized warming (C. J. Hollis et al., 2009) (Fig. 10b).

760 8 Conclusions

761 The Mg/Ca paleothermometer is complex. It is sensitive to multiple environmen-
 762 tal factors, which challenges both calibration and application. Traditionally, Mg/Ca ap-
 763 plications have “pre-corrected” the data for factors such as dissolution, laboratory clean-
 764 ing method, or pH sensitivity (e.g., Rosenthal & Lohmann, 2002; Evans et al., 2018; Gray
 765 & Evans, 2019). While effective, this makes uncertainty propagation challenging. A clear
 766 advantage of our BAYMAG models is that all known environmental sensitivities are in-
 767 cluded in a single model framework, making pre-correction obsolete. Furthermore, we
 768 show that we can account for most of the variance in the Mg/Ca of core top data through
 769 use of a hierarchical Bayesian model structure that leverages both culture and core top
 770 constraints on environmental sensitivities. Encouragingly, temperature remains the most
 771 important predictor of Mg/Ca, followed by bottom water calcite saturation state (Ω).
 772 Salinity and pH sensitivities are essentially undetectable in core top data; hence culture
 773 constraints are key.

774 The BAYMAG hierarchical models fit the data well, although some species, most
 775 notably *G. ruber*, still have trends in their residuals suggesting that some variance is left
 776 unexplained. Future work will be needed to identify why this is the case; we hypothe-
 777 size that there is latent co-variate that scales with temperature (possibly pH). Fortunately,
 778 the absolute magnitude of the residuals is small, such that the trends typically don’t bias
 779 predicted values. Indeed, applications of BAYMAG demonstrate that it yields reason-
 780 able forward predictions of Mg/Ca when compared to sediment trap observations, and
 781 reasonable inverse predictions when compared to independent SST proxies. The latter
 782 is true even though strong – and potentially incorrect – assumptions about past changes
 783 in Ω , salinity, and pH must be made. Deep time applications must additionally account
 784 for changing Mg/Ca_{sw}. We use independent constraints on the evolution of Mg/Ca_{sw}
 785 to develop a smoothed ensemble estimate for use with BAYMAG. Example applications
 786 once again suggest good agreement with independent SST proxies, but there can be large
 787 uncertainties in absolute SST estimates when potential changes in Ω in particular are
 788 considered.

789 In this work, we seek to develop prediction models for Mg/Ca of foraminifera that
 790 are independent from other proxy systems. However, given the multivariate nature of
 791 Mg/Ca, it would be beneficial to use information from other temperature proxies in a
 792 formal hierarchical model structure. Previous work has already explored this avenue by
 793 combining Mg/Ca measurements with TEX₈₆ or $\Delta 47$ to estimate Mg/Ca_{sw} (e.g., O’Brien
 794 et al., 2014; Evans, Brierley, et al., 2016; Evans et al., 2018) and by combining Mg/Ca
 795 with $\delta^{18}\text{O}$ to infer $\delta^{18}\text{O}_{sw}$ or salinity (e.g., Oppo et al., 2009; Thirumalai et al., 2016;
 796 Tierney et al., 2016). Future work might explore incorporating $\delta^{11}\text{B}$ and B/Ca estimates
 797 of pH and calcite saturation state, respectively. This would almost certainly improve past
 798 estimates of SST, especially over timescales when ocean carbonate chemistry is expected
 799 to have changed substantially.

800 Appendix A Bayesian regression model priors

801 Priors for the Bayesian regression parameters were chosen so as to enforce the ex-
 802 pected direction of the sensitivity based on geochemistry (e.g., Mg/Ca increases with tem-

803 perature but decreases with Ω^{-2}) but otherwise be only weakly informative, with the
 804 exception of the salinity prior. The salinity sensitivity was explicitly bounded by the pos-
 805 terior value for β_S from culture data ($4.3 \pm 1.3\%$, 2σ) to counteract the tendency of the
 806 core tops to dilute the sensitivity. Slightly different priors for the pooled and group-specific
 807 models were used for the $\sigma_{\beta T_c}$ and σ parameters:

$$\begin{aligned}
 808 \quad & \alpha \sim \mathcal{U}(-5, 10), \\
 809 \quad & \mu_{\beta T_c} \sim \mathcal{N}_{[0, \infty)}(0.07, 0.015), \\
 810 \quad & \sigma_{\beta T_c} \sim \text{HalfCauchy}(0.02)_{[\text{pooled}]}; \sim \text{HalfCauchy}(0.015)_{[\text{species}]} \\
 811 \quad & \beta_S \sim \mathcal{N}_{[0, \infty)}(0.043, 0.0065), \\
 812 \quad & \beta_P \sim \mathcal{N}_{(\infty, 0]}(-0.7, 0.2), \\
 813 \quad & \beta_O \sim \mathcal{N}_{(\infty, 0]}(-0.2, 0.2), \\
 814 \quad & \beta_C \sim \mathcal{N}_{[0, \infty)}(0.12, 0.1), \\
 815 \quad & \sigma \sim \mathcal{U}(0, 0.5)_{[\text{pooled}]}; \sim \mathcal{U}(0, 0.3)_{[\text{species}]} \tag{A1}
 \end{aligned}$$

816 Plots of the prior vs. posterior distributions for the pooled annual and group-specific sea-
 817 sonal models are shown below. Note that the temperature panel contains posteriors for
 818 the hyperparameter $\mu_{\beta T_c}$, the culture data parameter β_{T_c} , and the core top data param-
 819 eter β_T .

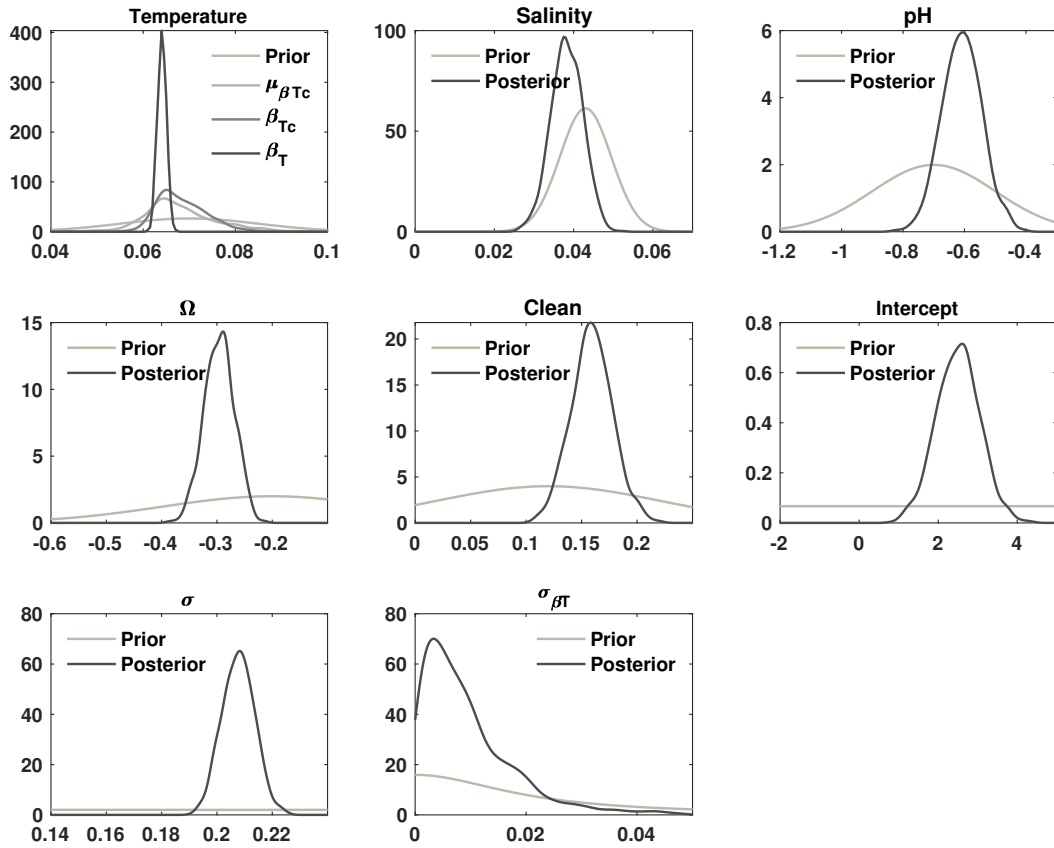


Figure A1. Prior and posterior parameter distributions for the pooled annual model.

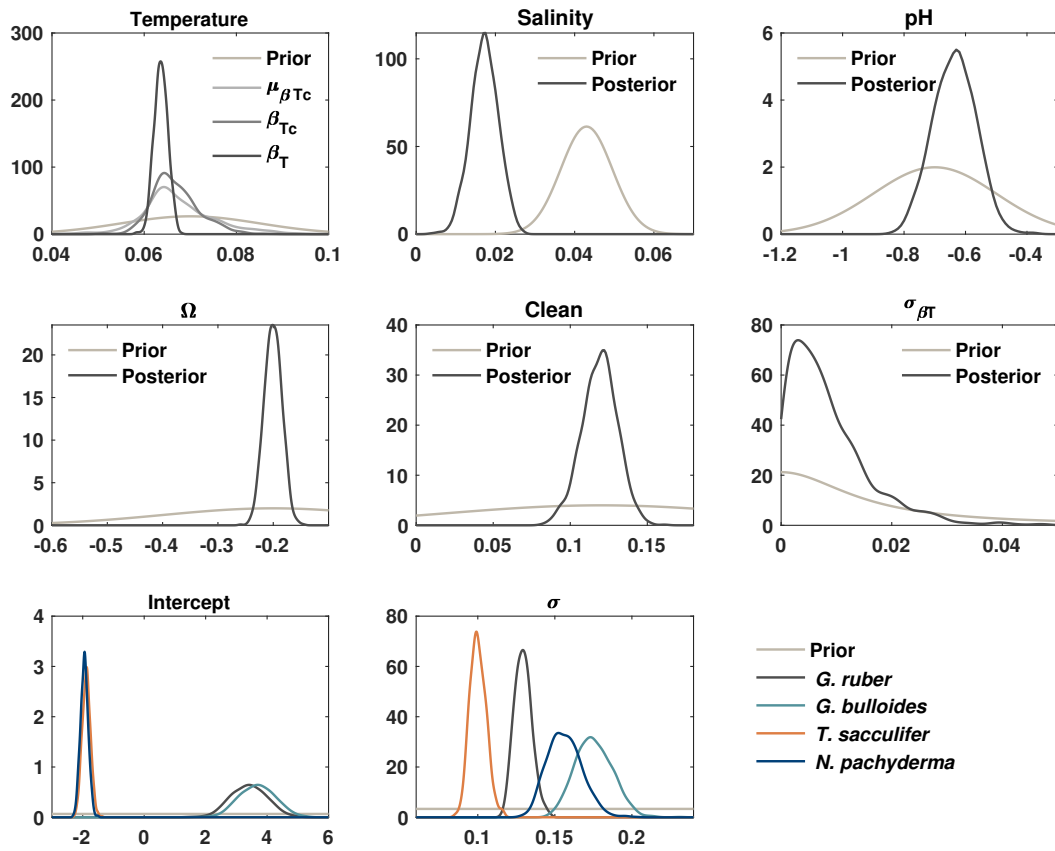


Figure A2. Prior and posterior parameter distributions for the group-specific seasonal model.

Acknowledgments

This work was supported by National Science Foundation grant AGS #1602301, Heising-Simons Foundation grant #2016-015, and the Packard Fellowship in Science and Engineering to JT. We thank Dr. David Evans, Dr. Jennifer Hertzberg, and one anonymous reviewer for valuable comments that improved the manuscript. BAYMAG code (in MATLAB) is available on GitHub: <https://github.com/jesstierney/BAYMAG>. Compiled core top, culture, and Mg/Ca of seawater data are available as Supplementary Data, as well as online in the Pangaea database at <https://doi.pangaea.de/10.1594/PANGAEA.908097>.

References

- Aagaard-Sørensen, S., Husum, K., Hald, M., Marchitto, T., & Godtliebse, F. (2014). Sub sea surface temperatures in the Polar North Atlantic during the Holocene: Planktic foraminiferal Mg/Ca temperature reconstructions. *The Holocene*, *24*(1), 93–103.
- Allen, K. A., Hönisch, B., Eggins, S. M., Haynes, L. L., Rosenthal, Y., & Yu, J. (2016). Trace element proxies for surface ocean conditions: A synthesis of culture calibrations with planktic foraminifera. *Geochimica et Cosmochimica Acta*, *193*, 197–221.
- Anand, P., Elderfield, H., & Conte, M. H. (2003). Calibration of Mg/Ca thermometry in planktonic foraminifera from a sediment trap time series. *Paleoceanography*, *18*(2).
- Arbuszewski, J., deMenocal, P., Kaplan, A., & Farmer, E. C. (2010). On the fidelity of shell-derived $\delta^{18}\text{O}$ seawater estimates. *Earth and Planetary Science Letters*, *300*(3), 185–196.
- Arbuszewski, J. A., Cléroux, C., Bradtmiller, L., & Mix, A. (2013). Meridional shifts of the Atlantic intertropical convergence zone since the Last Glacial Maximum. *Nature Geoscience*, *6*(11), 959–962.
- Aurahs, R., Treis, Y., Darling, K., & Kucera, M. (2011). A revised taxonomic and phylogenetic concept for the planktonic foraminifer species *Globigerinoides ruber* based on molecular and morphometric evidence. *Marine Micropaleontology*, *79*(1-2), 1–14.
- Baatsen, M., Van Hinsbergen, D. J., Heydt, A. S., Dijkstra, H. A., Sluijs, A., Abels, H. A., & Bijl, P. K. (2016). Reconstructing geographical boundary conditions for palaeoclimate modelling during the Cenozoic. *Climate of the Past*, *12*(8), 1635–1644.
- Barker, S., Cacho, I., Benway, H., & Tachikawa, K. (2005). Planktonic foraminiferal Mg/Ca as a proxy for past oceanic temperatures: a methodological overview and data compilation for the Last Glacial Maximum. *Quaternary Science Reviews*, *24*(7), 821–834.
- Barker, S., Greaves, M., & Elderfield, H. (2003). A study of cleaning procedures used for foraminiferal Mg/Ca paleothermometry. *Geochemistry, Geophysics, Geosystems*, *4*(9).
- Benway, H. M., Mix, A. C., Haley, B. A., & Klinkhammer, G. P. (2006). Eastern Pacific Warm Pool paleosalinity and climate variability: 0–30 kyr. *Paleoceanography*, *21*(3).
- Bereiter, B., Eggelston, S., Schmitt, J., Nehrbass-Ahles, C., Stocker, T. F., Fischer, H., . . . Chappellaz, J. (2015). Revision of the EPICA Dome C CO₂ record from 800 to 600 kyr before present. *Geophysical Research Letters*, *42*(2), 542–549.
- Berger, W. H. (1970). Planktonic foraminifera: selective solution and the lysocline. *Marine Geology*, *8*(2), 111–138.
- Bijl, P. K., Bendle, J. A., Bohaty, S. M., Pross, J., Schouten, S., Tauxe, L., . . . Expedition 318 Scientists (2013). Eocene cooling linked to early flow across the Tasmanian Gateway. *Proceedings of the National Academy of Sciences*,

- 873 110(24), 9645–9650.
- 874 Bijl, P. K., Schouten, S., Sluijs, A., Reichart, G.-J., Zachos, J. C., & Brinkhuis,
875 H. (2009). Early Palaeogene temperature evolution of the southwest Pacific
876 Ocean. *Nature*, 461(7265), 776–779.
- 877 Boussetta, S., Kallel, N., Bassinot, F., Labeyrie, L., Duplessy, J.-C., Caillon, N., ...
878 Rebaubier, H. (2012). Mg/Ca-paleothermometry in the western Mediterranean
879 Sea on planktonic foraminifer species *Globigerina bulloides*: Constraints and
880 implications. *Comptes Rendus Geoscience*, 344(5), 267–276.
- 881 Boyer, T. P., Antonov, J. I., Baranova, O. K., Coleman, C., Garcia, H. E., Grodsky,
882 A., ... Zweng, M. (2013). *World ocean database 2013* (Tech. Rep.). Silver
883 Spring, MD: NOAA.
- 884 Boyle, E., & Keigwin, L. (1985). Comparison of Atlantic and Pacific paleochemi-
885 cal records for the last 215,000 years: Changes in deep ocean circulation and
886 chemical inventories. *Earth and Planetary Science Letters*, 76(1), 135–150.
- 887 Brennan, S. T., Lowenstein, T. K., & Cendón, D. I. (2013). The major-ion compo-
888 sition of Cenozoic seawater: The past 36 million years from fluid inclusions in
889 marine halite. *American Journal of Science*, 313(8), 713–775.
- 890 Brown, S. J., & Elderfield, H. (1996). Variations in Mg/Ca and Sr/Ca ratios of
891 planktonic foraminifera caused by postdepositional dissolution: Evidence of
892 shallow Mg-dependent dissolution. *Paleoceanography*, 11(5), 543–551.
- 893 Carpenter, B., Gelman, A., Hoffman, M. D., Lee, D., Goodrich, B., Betancourt, M.,
894 ... Riddell, A. (2017). Stan: A probabilistic programming language. *Journal*
895 *of Statistical Software*, 76(1).
- 896 Cléroux, C., Cortijo, E., Anand, P., Labeyrie, L., Bassinot, F., Caillon, N., & Du-
897 plessy, J.-C. (2008). Mg/Ca and Sr/Ca ratios in planktonic foraminifera:
898 Proxies for upper water column temperature reconstruction. *Paleoceanography*
899 *and Paleoclimatology*, 23(3).
- 900 Coggon, R. M., Teagle, D. A., Smith-Duque, C. E., Alt, J. C., & Cooper, M. J.
901 (2010). Reconstructing past seawater Mg/Ca and Sr/Ca from mid-ocean ridge
902 flank calcium carbonate veins. *Science*, 327(5969), 1114–1117.
- 903 Cramwinckel, M. J., Huber, M., Kocken, I. J., Agnini, C., Bijl, P. K., Bohaty, S. M.,
904 ... Sluijs, A. (2018). Synchronous tropical and polar temperature evolution in
905 the Eocene. *Nature*, 559(7714), 382–386.
- 906 Dahl, K. A., & Oppo, D. W. (2006). Sea surface temperature pattern reconstruc-
907 tions in the Arabian Sea. *Paleoceanography*, 21(1).
- 908 Dai, Y., Yu, J., DeMenocal, P., & Hyams-Kaphzan, O. (2019). Influences of tem-
909 perature and secondary environmental parameters on planktonic foraminiferal
910 Mg/Ca: A new core-top calibration. *Geochemistry, Geophysics, Geosystems*,
911 20, 4370–4381.
- 912 Darling, K. F., Kucera, M., Kroon, D., & Wade, C. M. (2006). A resolution for the
913 coiling direction paradox in *Neogloboquadrina pachyderma*. *Paleoceanography*,
914 21(2).
- 915 Davis, C. V., Fehrenbacher, J. S., Hill, T. M., Russell, A. D., & Spero, H. J. (2017).
916 Relationships Between Temperature, pH, and Crusting on Mg/Ca Ratios in
917 Laboratory-Grown *Neogloboquadrina Foraminifera*. *Paleoceanography*, 32(11),
918 1137–1152.
- 919 de Garidel-Thoron, T., Rosenthal, Y., Beaufort, L., Bard, E., Sonzogni, C., & Mix,
920 A. C. (2007). A multiproxy assessment of the western equatorial Pacific
921 hydrography during the last 30 kyr. *Paleoceanography*, 22(3).
- 922 Dekens, P. S., Lea, D. W., Pak, D. K., & Spero, H. J. (2002). Core top calibration
923 of Mg/Ca in tropical foraminifera: Refining paleotemperature estimation. *Geo-*
924 *chemistry, Geophysics, Geosystems*, 3(4), 1–29.
- 925 Delaney, M. L., Bé, A. W., & Boyle, E. A. (1985). Li, Sr, Mg, and Na in
926 foraminiferal calcite shells from laboratory culture, sediment traps, and sed-
927 iment cores. *Geochimica et Cosmochimica Acta*, 49(6), 1327–1341.

- 928 De Nooijer, L., Van Dijk, I., Toyofuku, T., & Reichert, G. (2017). The impacts
929 of seawater Mg/Ca and temperature on element incorporation in benthic
930 foraminiferal calcite. *Geochemistry, Geophysics, Geosystems*, 18(10), 3617–
931 3630.
- 932 Dickson, A., & Millero, F. J. (1987). A comparison of the equilibrium constants for
933 the dissociation of carbonic acid in seawater media. *Deep Sea Research Part A.*
934 *Oceanographic Research Papers*, 34(10), 1733–1743.
- 935 Dickson, J. (2002). Fossil echinoderms as monitor of the Mg/Ca ratio of Phanerozoic
936 oceans. *Science*, 298(5596), 1222–1224.
- 937 Dickson, J. (2004). Echinoderm skeletal preservation: calcite-aragonite seas and the
938 Mg/Ca ratio of Phanerozoic oceans. *Journal of Sedimentary Research*, 74(3),
939 355–365.
- 940 Dueñas-Bohórquez, A., da Rocha, R. E., Kuroyanagi, A., Bijma, J., & Reichert, G.-
941 J. (2009). Effect of salinity and seawater calcite saturation state on Mg and Sr
942 incorporation in cultured planktonic foraminifera. *Marine Micropaleontology*,
943 73(3), 178–189.
- 944 Dunlea, A. G., Murray, R. W., Ramos, D. P. S., & Higgins, J. A. (2017). Cenozoic
945 global cooling and increased seawater Mg/Ca via reduced reverse weathering.
946 *Nature Communications*, 8(1).
- 947 Dyez, K. A., Zahn, R., & Hall, I. R. (2014). Multicentennial Agulhas leakage vari-
948 ability and links to North Atlantic climate during the past 80,000 years. *Paleo-*
949 *ceanography*, 29(12), 1238–1248.
- 950 Elderfield, H., & Ganssen, G. (2000). Past temperature and $\delta^{18}\text{O}$ of surface ocean
951 waters inferred from foraminiferal Mg/Ca ratios. *Nature*, 405(6785), 442–445.
- 952 Elderfield, H., Vautravers, M., & Cooper, M. (2002). The relationship between shell
953 size and Mg/Ca, Sr/Ca, $\delta^{18}\text{O}$, and $\delta^{13}\text{C}$ of species of planktonic foraminifera.
954 *Geochemistry, Geophysics, Geosystems*, 3(8), 1–13.
- 955 Erez, J., & Honjo, S. (1981). Comparison of isotopic composition of planktonic
956 foraminifera in plankton tows, sediment traps and sediments. *Palaeogeography,*
957 *Palaeoclimatology, Palaeoecology*, 33(1-3), 129–156.
- 958 Evans, D., Brierley, C., Raymo, M. E., Erez, J., & Müller, W. (2016). Plank-
959 tic foraminifera shell chemistry response to seawater chemistry: Pliocene–
960 Pleistocene seawater Mg/Ca, temperature and sea level change. *Earth and*
961 *Planetary Science Letters*, 438, 139–148.
- 962 Evans, D., Erez, J., Oron, S., & Müller, W. (2015). Mg/Ca-temperature and
963 seawater-test chemistry relationships in the shallow-dwelling large benthic
964 foraminifera *Operculina ammonoides*. *Geochimica et Cosmochimica Acta*, 148,
965 325–342.
- 966 Evans, D., & Müller, W. (2012). Deep time foraminifera Mg/Ca paleothermometry:
967 Nonlinear correction for secular change in seawater Mg/Ca. *Paleoceanography*
968 *and Paleoclimatology*, 27(4).
- 969 Evans, D., Sagoo, N., Renema, W., Cotton, L. J., Müller, W., Todd, J. A., . . . Af-
970 fek, H. P. (2018). Eocene greenhouse climate revealed by coupled clumped
971 isotope-Mg/Ca thermometry. *Proceedings of the National Academy of Sci-*
972 *ences*, 201714744.
- 973 Evans, D., Wade, B. S., Henahan, M., Erez, J., & Müller, W. (2016). Revisiting
974 carbonate chemistry controls on planktic foraminifera Mg/Ca: implications for
975 sea surface temperature and hydrology shifts over the Paleocene–Eocene Ther-
976 mal Maximum and Eocene–Oligocene transition. *Climate of the Past*, 12(4),
977 819–835.
- 978 Fairbanks, R. G., Wiebe, P. H., & Bé, A. W. (1980). Vertical distribution and
979 isotopic composition of living planktonic foraminifera in the western North
980 Atlantic. *Science*, 207(4426), 61–63.
- 981 Fallet, U., Castañeda, I. S., Henry-Edwards, A., Richter, T. O., Boer, W., Schouten,
982 S., & Brummer, G.-J. (2012). Sedimentation and burial of organic and in-

- 983 organic temperature proxies in the Mozambique Channel, SW Indian Ocean.
 984 *Deep Sea Research Part I: Oceanographic Research Papers*, 59, 37–53.
- 985 Farmer, E. C., Demenocal, P. B., & Marchitto, T. M. (2005). Holocene and deglacial
 986 ocean temperature variability in the Benguela upwelling region: Implications
 987 for low-latitude atmospheric circulation. *Paleoceanography*, 20(2).
- 988 Ferguson, J., Henderson, G., Kucera, M., & Rickaby, R. (2008). Systematic change
 989 of foraminiferal Mg/Ca ratios across a strong salinity gradient. *Earth and
 990 Planetary Science Letters*, 265(1), 153–166.
- 991 Filippova, A., Kienast, M., Frank, M., & Schneider, R. (2016). Alkenone paleother-
 992 mometry in the North Atlantic: A review and synthesis of surface sediment
 993 data and calibrations. *Geochemistry, Geophysics, Geosystems*, 17(4), 1370–
 994 1382.
- 995 Friedrich, O., Schiebel, R., Wilson, P. A., Weldeab, S., Beer, C. J., Cooper, M. J., &
 996 Fiebig, J. (2012). Influence of test size, water depth, and ecology on Mg/Ca,
 997 Sr/Ca, $\delta^{18}\text{O}$ and $\delta^{13}\text{C}$ in nine modern species of planktic foraminifers. *Earth
 998 and Planetary Science Letters*, 319, 133–145.
- 999 Ganssen, G., & Kroon, D. (2000). The isotopic signature of planktonic foraminifera
 1000 from NE Atlantic surface sediments: implications for the reconstruction of past
 1001 oceanic conditions. *Journal of the Geological Society*, 157(3), 693–699.
- 1002 Gebregiorgis, D., Hathorne, E. C., Sijinkumar, A., Nath, B. N., Nürnberg, D., &
 1003 Frank, M. (2016). South Asian summer monsoon variability during the last
 1004 ~54 kyrs inferred from surface water salinity and river runoff proxies. *Quater-
 1005 nary Science Reviews*, 138, 6–15.
- 1006 Gelman, A., Carlin, J., Stern, H., & Rubin, D. (2003). *Bayesian data analysis* (2nd
 1007 ed.). Boca Raton: Chapman & Hall/CRC.
- 1008 Gibbons, F. T., Oppo, D. W., Mohtadi, M., Rosenthal, Y., Cheng, J., Liu, Z., &
 1009 Linsley, B. K. (2014). Deglacial $\delta^{18}\text{O}$ and hydrologic variability in the trop-
 1010 ical Pacific and Indian Oceans. *Earth and Planetary Science Letters*, 387,
 1011 240–251.
- 1012 Gothmann, A. M., Stolarski, J., Adkins, J. F., Schoene, B., Dennis, K. J., Schrag,
 1013 D. P., . . . Bender, M. L. (2015). Fossil corals as an archive of secular varia-
 1014 tions in seawater chemistry since the Mesozoic. *Geochimica et Cosmochimica
 1015 Acta*, 160, 188–208.
- 1016 Gray, W. R., & Evans, D. (2019). Non-thermal influences on Mg/Ca in plank-
 1017 tonic foraminifera: A review of culture studies and application to the Last
 1018 Glacial Maximum. *Paleoceanography and Paleoclimatology*, 34. doi:
 1019 <https://doi.org/10.1029/2018PA003517>
- 1020 Gray, W. R., Weldeab, S., Lea, D. W., Rosenthal, Y., Gruber, N., Donner, B., &
 1021 Fischer, G. (2018). The effects of temperature, salinity, and the carbonate
 1022 system on Mg/Ca in *Globigerinoides ruber* (white): A global sediment trap
 1023 calibration. *Earth and Planetary Science Letters*, 482, 607–620.
- 1024 Hakim, G. J., Emile-Geay, J., Steig, E. J., Noone, D., Anderson, D. M., Tardif, R.,
 1025 . . . Perkins, W. A. (2016). The last millennium climate reanalysis project:
 1026 Framework and first results. *Journal of Geophysical Research: Atmospheres*,
 1027 121(12), 6745–6764.
- 1028 Hastings, D. W., Russell, A. D., & Emerson, S. R. (1998). Foraminiferal magne-
 1029 sium in *Globigerinoides sacculifer* as a paleotemperature proxy. *Paleoceanogra-
 1030 phy and Paleoclimatology*, 13(2), 161–169.
- 1031 Hauzer, H., Evans, D., Müller, W., Rosenthal, Y., & Erez, J. (2018). Calibration
 1032 of Na partitioning in the calcitic foraminifer *Operculina ammonoides* under
 1033 variable Ca concentration: Toward reconstructing past seawater composition.
 1034 *Earth and Planetary Science Letters*, 497, 80–91.
- 1035 Herold, N., Buzan, J., Seton, M., Goldner, A., Green, J., Müller, R., . . . Huber, M.
 1036 (2014). A suite of early Eocene (~55 Ma) climate model boundary conditions.
 1037 *Geoscientific Model Development*, 7(5), 2077–2090.

- 1038 Hertzberg, J. E., & Schmidt, M. W. (2013). Refining *Globigerinoides ruber* Mg/Ca
1039 paleothermometry in the Atlantic Ocean. *Earth and Planetary Science Letters*,
1040 *383*, 123–133.
- 1041 Higgins, J. A., & Schrag, D. P. (2015). The Mg isotopic composition of Cenozoic
1042 seawater—evidence for a link between Mg-clays, seawater Mg/Ca, and climate.
1043 *Earth and Planetary Science Letters*, *416*, 73–81.
- 1044 Hines, B. R., Hollis, C. J., Atkins, C. B., Baker, J. A., Morgans, H. E., & Strong,
1045 P. C. (2017). Reduction of oceanic temperature gradients in the early eocene
1046 southwest pacific ocean. *Palaeogeography, palaeoclimatology, palaeoecology*,
1047 *475*, 41–54.
- 1048 Hollis, C., Dunkley Jones, T., Anagnostou, E., Bijl, P., Cramwinckel, M., Cui, Y.,
1049 ... Lunt, D. (2019). The DeepMIP contribution to PMIP4: methodologies
1050 for selection, compilation and analysis of latest Paleocene and early Eocene
1051 climate proxy data, incorporating version 0.1 of the DeepMIP database. *Geo-*
1052 *scientific Model Development Discussions*.
- 1053 Hollis, C. J., Handley, L., Crouch, E. M., Morgans, H. E., Baker, J. A., Creech, J.,
1054 ... Pancost, R. (2009). Tropical sea temperatures in the high-latitude South
1055 Pacific during the Eocene. *Geology*, *37*(2), 99–102.
- 1056 Hollis, C. J., Taylor, K. W., Handley, L., Pancost, R. D., Huber, M., Creech, J. B.,
1057 ... Zachos, J. C. (2012). Early Paleogene temperature history of the South-
1058 west Pacific Ocean: Reconciling proxies and models. *Earth and Planetary*
1059 *Science Letters*, *349*, 53–66.
- 1060 Hollstein, M., Mohtadi, M., Rosenthal, Y., Moffa Sanchez, P., Oppo, D.,
1061 Martínez Méndez, G., ... Hebbeln, D. (2017). Stable oxygen isotopes and
1062 Mg/Ca in Planktic foraminifera from modern surface sediments of the Western
1063 Pacific Warm Pool: Implications for thermocline reconstructions. *Paleoceanog-*
1064 *raphy*, *32*(11), 1174–1194.
- 1065 Hönisch, B., Allen, K. A., Lea, D. W., Spero, H. J., Eggins, S. M., Arbuszewski,
1066 J., ... Elderfield, H. (2013). The influence of salinity on Mg/Ca in planktic
1067 foraminifers—Evidence from cultures, core-top sediments and complementary
1068 $\delta^{18}\text{O}$. *Geochimica et Cosmochimica Acta*, *121*, 196–213.
- 1069 Horita, J., Zimmermann, H., & Holland, H. D. (2002). Chemical evolution of seawater
1070 during the Phanerozoic: Implications from the record of marine evaporites.
1071 *Geochimica et Cosmochimica Acta*, *66*(21), 3733–3756.
- 1072 Inglis, G. N., Farnsworth, A., Lunt, D., Foster, G. L., Hollis, C. J., Pagani, M., ...
1073 Pancost, R. (2015). Descent toward the Icehouse: Eocene sea surface cooling
1074 inferred from GDGT distributions. *Paleoceanography*, *30*(7), 1000–1020.
- 1075 Johnstone, H. J., Yu, J., Elderfield, H., & Schulz, M. (2011). Improving temperature
1076 estimates derived from Mg/Ca of planktonic foraminifera using X-ray com-
1077 puted tomography-based dissolution index, XDX. *Paleoceanography*, *26*(1).
- 1078 Keigwin, L. D., Sachs, J. P., Rosenthal, Y., & Boyle, E. A. (2005). The 8200 year
1079 BP event in the slope water system, western subpolar North Atlantic. *Paleo-*
1080 *ceanography*, *20*(2).
- 1081 Khider, D., Huerta, G., Jackson, C., Stott, L., & Emile-Geay, J. (2015). A Bayesian,
1082 multivariate calibration for *Globigerinoides ruber* Mg/Ca. *Geochemistry, Geo-*
1083 *physics, Geosystems*, *16*(9), 2916–2932.
- 1084 Kienast, M., MacIntyre, G., Dubois, N., Higginson, S., Normandeau, C., Chazen, C.,
1085 & Herbert, T. (2012). Alkenone unsaturation in surface sediments from the
1086 eastern equatorial Pacific: Implications for SST reconstructions. *Paleoceanogra-*
1087 *phy*, *27*(1).
- 1088 Kisakürek, B., Eisenhauer, A., Böhm, F., Garbe-Schönberg, D., & Erez, J. (2008).
1089 Controls on shell Mg/Ca and Sr/Ca in cultured planktonic foraminiferan,
1090 *Globigerinoides ruber* (white). *Earth and Planetary Science Letters*, *273*,
1091 260–269.
- 1092 Kozdon, R., Eisenhauer, A., Weinelt, M., Meland, M. Y., & Nürnberg, D. (2009).

- 1093 Reassessing Mg/Ca temperature calibrations of *Neogloboquadrina pachyderma*
 1094 (sinistral) using paired $\delta^{44/40}\text{Ca}$ and Mg/Ca measurements. *Geochemistry,*
 1095 *Geophysics, Geosystems, 10*(3).
- 1096 Kristjánsson, G. B., Moros, M., Andrews, J. T., & Jennings, A. E. (2017).
 1097 Holocene Mg/Ca, alkenones, and light stable isotope measurements on the
 1098 outer North Iceland shelf (MD99-2269): A comparison with other multi-proxy
 1099 data and sub-division of the Holocene. *The Holocene, 27*(1), 52–62.
- 1100 Kubota, Y., Kimoto, K., Tada, R., Oda, H., Yokoyama, Y., & Matsuzaki, H. (2010).
 1101 Variations of East Asian summer monsoon since the last deglaciation based on
 1102 Mg/Ca and oxygen isotope of planktic foraminifera in the northern East China
 1103 Sea. *Paleoceanography and Paleoclimatology, 25*(4).
- 1104 Lauvset, S. K., Key, R. M., Olsen, A., van Heuven, S., Velo, A., Lin, X., ... Wa-
 1105 telet, S. (2016). A new global interior ocean mapped climatology: the 1×1
 1106 GLODAP version 2. *Earth System Science Data, 8*, 325–340.
- 1107 Lea, D. W., Mashiotta, T. A., & Spero, H. J. (1999). Controls on magnesium and
 1108 strontium uptake in planktonic foraminifera determined by live culturing.
 1109 *Geochimica et Cosmochimica Acta, 63*(16), 2369–2379.
- 1110 Lea, D. W., Pak, D. K., Belanger, C. L., Spero, H. J., Hall, M. A., & Shackleton,
 1111 N. J. (2006). Paleoclimate history of Galapagos surface waters over the last
 1112 135,000 yr. *Quaternary Science Reviews, 25*(11-12), 1152–1167.
- 1113 Lea, D. W., Pak, D. K., Peterson, L. C., & Hughen, K. A. (2003). Synchronicity of
 1114 tropical and high-latitude Atlantic temperatures over the last glacial termina-
 1115 tion. *science, 301*(5638), 1361–1364.
- 1116 Lea, D. W., Pak, D. K., & Spero, H. J. (2000). Climate impact of late Quater-
 1117 nary equatorial Pacific sea surface temperature variations. *Science, 289*(5485),
 1118 1719–1724.
- 1119 Leduc, G., Vidal, L., Tachikawa, K., Rostek, F., Sonzogni, C., Beaufort, L., & Bard,
 1120 E. (2007). Moisture transport across Central America as a positive feedback
 1121 on abrupt climatic changes. *Nature, 445*(7130), 908–911.
- 1122 Levi, C., Labeyrie, L., Bassinot, F., Guichard, F., Cortijo, E., Waelbroeck, C., ...
 1123 Elderfield, H. (2007). Low-latitude hydrological cycle and rapid climate
 1124 changes during the last deglaciation. *Geochemistry, Geophysics, Geosystems,*
 1125 *8*(5).
- 1126 Linsley, B. K., Rosenthal, Y., & Oppo, D. W. (2010). Holocene evolution of the In-
 1127 donesian throughflow and the western Pacific warm pool. *Nature Geoscience,*
 1128 *3*(8), 578.
- 1129 Lombard, F., Labeyrie, L., Michel, E., Bopp, L., Cortijo, E., Retailliau, S., ... Joris-
 1130 sen, F. (2011). Modelling planktic foraminifer growth and distribution using
 1131 an ecophysiological multi-species approach. *Biogeosciences, 8*(4), 853–873.
- 1132 Lombard, F., Labeyrie, L., Michel, E., Spero, H. J., & Lea, D. W. (2009). Modelling
 1133 the temperature dependent growth rates of planktic foraminifera. *Marine Mi-
 1134 cropaleontology, 70*(1-2), 1–7.
- 1135 Lowenstein, T. K., Timofeeff, M. N., Brennan, S. T., Hardie, L. A., & Demicco,
 1136 R. V. (2001). Oscillations in Phanerozoic seawater chemistry: Evidence from
 1137 fluid inclusions. *Science, 294*(5544), 1086–1088.
- 1138 Malevich, S., Vetter, L., & Tierney, J. (2019). Global core top calibration of $\delta^{18}\text{O}$
 1139 in planktic foraminifera to sea-surface temperature. *Paleoceanography, 34*(8),
 1140 1292–1315.
- 1141 Marchitto, T. M., Muscheler, R., Ortiz, J. D., Carriquiry, J. D., & van Geen, A.
 1142 (2010). Dynamical response of the tropical Pacific Ocean to solar forcing
 1143 during the early Holocene. *Science, 330*(6009), 1378–1381.
- 1144 Mashiotta, T. A., Lea, D. W., & Spero, H. J. (1999). Glacial-interglacial changes in
 1145 Subantarctic sea surface temperature and $\delta^{18}\text{O}$ -water using foraminiferal Mg.
 1146 *Earth and Planetary Science Letters, 170*(4), 417–432.
- 1147 Mathien-Blard, E., & Bassinot, F. (2009). Salinity bias on the foraminifera Mg/Ca

- 1148 thermometry: Correction procedure and implications for past ocean hydro-
 1149 graphic reconstructions. *Geochemistry, Geophysics, Geosystems*, 10(12).
- 1150 McConnell, M. C., & Thunell, R. C. (2005). Calibration of the planktonic
 1151 foraminiferal Mg/Ca paleothermometer: Sediment trap results from the Guay-
 1152 mas Basin, Gulf of California. *Paleoceanography and Paleoclimatology*, 20(2).
- 1153 Meland, M. Y., Jansen, E., Elderfield, H., Dokken, T. M., Olsen, A., & Bellerby,
 1154 R. G. (2006). Mg/Ca ratios in the planktonic foraminifer *Neogloboquadrina*
 1155 *pachyderma* (sinistral) in the northern North Atlantic/Nordic Seas. *Geochem-*
 1156 *istry, Geophysics, Geosystems*, 7(6).
- 1157 Mewes, A., Langer, G., de Nooijer, L. J., Bijma, J., & Reichart, G.-J. (2014). Ef-
 1158 fect of different seawater Mg²⁺ concentrations on calcification in two benthic
 1159 foraminifers. *Marine Micropaleontology*, 113, 56–64.
- 1160 Moffa-Sánchez, P., Hall, I. R., Barker, S., Thornalley, D. J., & Yashayaev, I. (2014).
 1161 Surface changes in the eastern Labrador Sea around the onset of the Little Ice
 1162 Age. *Paleoceanography*, 29(3), 160–175.
- 1163 Mohtadi, M., Oppo, D. W., Lückge, A., DePol-Holz, R., Steinke, S., Groeneveld, J.,
 1164 ... Hebbeln, D. (2011). Reconstructing the thermal structure of the upper
 1165 ocean: Insights from planktic foraminifera shell chemistry and alkenones in
 1166 modern sediments of the tropical eastern Indian Ocean. *Paleoceanography and*
 1167 *Paleoclimatology*, 26(3).
- 1168 Mohtadi, M., Steinke, S., Groeneveld, J., Fink, H. G., Rixen, T., Hebbeln, D., ...
 1169 Herunadi, B. (2009). Low-latitude control on seasonal and interannual changes
 1170 in planktonic foraminiferal flux and shell geochemistry off south Java: A sedi-
 1171 ment trap study. *Paleoceanography*, 24(1).
- 1172 Mohtadi, M., Steinke, S., Lückge, A., Groeneveld, J., & Hathorne, E. C. (2010).
 1173 Glacial to Holocene surface hydrography of the tropical eastern Indian Ocean.
 1174 *Earth and Planetary Science Letters*, 292(1), 89–97.
- 1175 Morley, A., Babila, T. L., Wright, J., Ninnemann, U., Kleiven, K., Irvani, N., &
 1176 Rosenthal, Y. (2017). Environmental Controls on Mg/Ca in *Neogloboquadrina*
 1177 *incompta*: A Core-Top Study From the Subpolar North Atlantic. *Geochem-*
 1178 *istry, Geophysics, Geosystems*, 18(12), 4276–4298.
- 1179 Mortyn, P. G., & Charles, C. D. (2003). Planktonic foraminiferal depth habitat
 1180 and $\delta^{18}\text{O}$ calibrations: Plankton tow results from the Atlantic sector of the
 1181 Southern Ocean. *Paleoceanography*, 18(2).
- 1182 Mucci, A., & Morse, J. W. (1983). The incorporation of Mg²⁺ and Sr²⁺ into calcite
 1183 overgrowths: influences of growth rate and solution composition. *Geochimica et*
 1184 *Cosmochimica Acta*, 47(2), 217–233.
- 1185 Nürnberg, D., Bijma, J., & Hemleben, C. (1996). Assessing the reliability of magne-
 1186 sium in foraminiferal calcite as a proxy for water mass temperatures. *Geochim-*
 1187 *ica et Cosmochimica Acta*, 60(5), 803–814.
- 1188 Nürnberg, D., Ziegler, M., Karas, C., Tiedemann, R., & Schmidt, M. W. (2008).
 1189 Interacting Loop Current variability and Mississippi River discharge over the
 1190 past 400 kyr. *Earth and Planetary Science Letters*, 272(1-2), 278–289.
- 1191 O’Brien, C. L., Foster, G. L., Martínez-Botí, M. A., Abell, R., Rae, J. W., & Pan-
 1192 cost, R. D. (2014). High sea surface temperatures in tropical warm pools
 1193 during the Pliocene. *Nature Geoscience*, 7(8), 606–611.
- 1194 Oomori, T., Kaneshima, H., Maezato, Y., & Kitano, Y. (1987). Distribution coeffi-
 1195 cient of Mg²⁺ ions between calcite and solution at 10–50°C. *Marine Chemistry*,
 1196 20(4), 327–336.
- 1197 Oppo, D. W., Rosenthal, Y., & Linsley, B. K. (2009). 2,000-year-long tempera-
 1198 ture and hydrology reconstructions from the Indo-Pacific warm pool. *Nature*,
 1199 460(7259), 1113–1116.
- 1200 Oppo, D. W., & Sun, Y. (2005). Amplitude and timing of sea-surface tempera-
 1201 ture change in the northern South China Sea: Dynamic link to the East Asian
 1202 monsoon. *Geology*, 33(10), 785–788.

- 1203 Pahnke, K., Zahn, R., Elderfield, H., & Schulz, M. (2003). 340,000-year centennial-
1204 scale marine record of Southern Hemisphere climatic oscillation. *Science*,
1205 *301*(5635), 948–952.
- 1206 Palmer, M., & Pearson, P. N. (2003). A 23,000-year record of surface water pH and
1207 pCO₂ in the western equatorial Pacific Ocean. *Science*, *300*(5618), 480–482.
- 1208 Parker, A. O., Schmidt, M. W., Jobe, Z. R., & Slowey, N. C. (2016). A new per-
1209 spective on West African hydroclimate during the last deglaciation. *Earth and*
1210 *Planetary Science Letters*, *449*, 79–88.
- 1211 Pearson, P. N., van Dongen, B. E., Nicholas, C. J., Pancost, R. D., Schouten, S.,
1212 Singano, J. M., & Wade, B. S. (2007). Stable warm tropical climate through
1213 the Eocene Epoch. *Geology*, *35*(3), 211–214.
- 1214 Raitzsch, M., Dueñas-Bohórquez, A., Reichart, G.-J., de Nooijer, L. J., & Bickert, T.
1215 (2010). Incorporation of Mg and Sr in calcite of cultured benthic foraminifera:
1216 impact of calcium concentration and associated calcite saturation state. *Bio-*
1217 *geosciences*, *7*(3), 869–881.
- 1218 Ravelo, A., & Fairbanks, R. (1992). Oxygen isotopic composition of multiple species
1219 of planktonic foraminifera: Recorders of the modern photic zone temperature
1220 gradient. *Paleoceanography and Paleoclimatology*, *7*(6), 815–831.
- 1221 Regenberg, M., Nürnberg, D., Steph, S., Groeneveld, J., Garbe-Schönberg, D.,
1222 Tiedemann, R., & Dullo, W.-C. (2006). Assessing the effect of dissolution
1223 on planktonic foraminiferal Mg/Ca ratios: Evidence from Caribbean core tops.
1224 *Geochemistry, Geophysics, Geosystems*, *7*(7).
- 1225 Regenberg, M., Regenberg, A., Garbe-Schönberg, D., & Lea, D. W. (2014). Global
1226 dissolution effects on planktonic foraminiferal Mg/Ca ratios controlled by the
1227 calcite-saturation state of bottom waters. *Paleoceanography*, *29*(3), 127–142.
- 1228 Regenberg, M., Steph, S., Nürnberg, D., Tiedemann, R., & Garbe-Schönberg, D.
1229 (2009). Calibrating Mg/Ca ratios of multiple planktonic foraminiferal species
1230 with $\delta^{18}\text{O}$ -calcification temperatures: Paleothermometry for the upper water
1231 column. *Earth and Planetary Science Letters*, *278*(3-4), 324–336.
- 1232 Reynolds, L. A., & Thunell, R. C. (1986). Seasonal production and morphologic
1233 variation of *Neogloboquadrina pachyderma* (Ehrenberg) in the northeast Pa-
1234 cific. *Micropaleontology*, *32*, 1–18.
- 1235 Richey, J. N., Poore, R. Z., Flower, B. P., & Hollander, D. J. (2012). Ecological con-
1236 trols on the shell geochemistry of pink and white *Globigerinoides ruber* in the
1237 northern Gulf of Mexico: Implications for paleoceanographic reconstruction.
1238 *Marine Micropaleontology*, *82-83*(C), 28–37.
- 1239 Richey, J. N., Poore, R. Z., Flower, B. P., & Quinn, T. M. (2007). 1400 yr multi-
1240 proxy record of climate variability from the northern Gulf of Mexico. *Geology*,
1241 *35*(5), 423–426.
- 1242 Richey, J. N., Poore, R. Z., Flower, B. P., Quinn, T. M., & Hollander, D. J. (2009).
1243 Regionally coherent Little Ice Age cooling in the Atlantic warm pool. *Geophys-*
1244 *ical Research Letters*, *36*(21).
- 1245 Richey, J. N., Thirumalai, K., Khider, D., Reynolds, C. E., Partin, J. W., & Quinn,
1246 T. M. (2019). Considerations for *Globigerinoides ruber* (White and Pink)
1247 Paleoceanography: Comprehensive Insights From a Long-Running Sediment
1248 Trap. *Paleoceanography and Paleoclimatology*, *34*, 353–373.
- 1249 Riethdorf, J.-R., Max, L., Nürnberg, D., Lembke-Jene, L., & Tiedemann, R. (2013).
1250 Deglacial development of (sub) sea surface temperature and salinity in the
1251 subarctic northwest Pacific: Implications for upper-ocean stratification. *Paleo-*
1252 *ceanography*, *28*(1), 91–104.
- 1253 Romahn, S., Mackensen, A., Groeneveld, J., & Pätzold, J. (2014). Deglacial inter-
1254 mediate water reorganization: new evidence from the Indian Ocean. *Climate of*
1255 *the Past*, *10*(1), 293–303.
- 1256 Rosenthal, Y., & Boyle, E. A. (1993). Factors controlling the fluoride content of
1257 planktonic foraminifera: An evaluation of its paleoceanographic applicability.

- 1258 *Geochimica et Cosmochimica Acta*, 57(2), 335–346.
- 1259 Rosenthal, Y., Lohmann, G., Lohmann, K., & Sherrell, R. (2000). Incorporation
1260 and preservation of Mg in *Globigerinoides sacculifer*: Implications for recon-
1261 structing the temperature and $^{18}\text{O}/^{16}\text{O}$ of seawater. *Paleoceanography*, 15(1),
1262 135–145.
- 1263 Rosenthal, Y., & Lohmann, G. P. (2002). Accurate estimation of sea surface temper-
1264 atures using dissolution-corrected calibrations for Mg/Ca paleothermometry.
1265 *Paleoceanography*, 17(3).
- 1266 Rosenthal, Y., Oppo, D. W., & Linsley, B. K. (2003). The amplitude and phasing of
1267 climate change during the last deglaciation in the Sulu Sea, western equatorial
1268 Pacific. *Geophysical Research Letters*, 30(8).
- 1269 Rosenthal, Y., Perron-Cashman, S., Lear, C. H., Bard, E., Barker, S., Billups, K.,
1270 ... Wilson, P. A. (2004). Interlaboratory comparison study of Mg/Ca and
1271 Sr/Ca measurements in planktonic foraminifera for paleoceanographic research.
1272 *Geochemistry, Geophysics, Geosystems*, 5(4).
- 1273 Russell, A. D., Emerson, S., Nelson, B. K., Erez, J., & Lea, D. W. (1994). Ura-
1274 nium in foraminiferal calcite as a recorder of seawater uranium concentrations.
1275 *Geochimica et Cosmochimica Acta*, 58(2), 671–681.
- 1276 Russell, A. D., Hönisch, B., Spero, H. J., & Lea, D. W. (2004). Effects of seawater
1277 carbonate ion concentration and temperature on shell U, Mg, and Sr in
1278 cultured planktonic foraminifera. *Geochimica et Cosmochimica Acta*, 68(21),
1279 4347–4361.
- 1280 Rustic, G. T., Koutavas, A., Marchitto, T. M., & Linsley, B. K. (2015). Dynamical
1281 excitation of the tropical Pacific Ocean and ENSO variability by Little Ice Age
1282 cooling. *Science*, 350, 1537–1541.
- 1283 Sabbatini, A., Bassinot, F., Boussetta, S., Negri, A., Rebaubier, H., Dewilde, F., ...
1284 Morigi, C. (2011). Further constraints on the diagenetic influences and salinity
1285 effect on *Globigerinoides ruber* (white) Mg/Ca thermometry: Implications in
1286 the Mediterranean Sea. *Geochemistry, Geophysics, Geosystems*, 12(10).
- 1287 Sadekov, A. Y., Darling, K. F., Ishimura, T., Wade, C. M., Kimoto, K., Singh,
1288 A. D., ... others (2016). Geochemical imprints of genotypic variants of *Glo-*
1289 *bigerina bulloides* in the Arabian Sea. *Paleoceanography*, 31(10), 1440–1452.
- 1290 Saenger, C. P., & Evans, M. N. (2019). Calibration and validation of environmen-
1291 tal controls on planktic foraminifera Mg/Ca using global coretop data. *Paleo-*
1292 *ceanography and Paleoclimatology*, 34(8), 1249–1270.
- 1293 Saraswat, R., Lea, D. W., Nigam, R., Mackensen, A., & Naik, D. K. (2013).
1294 Deglaciation in the tropical Indian Ocean driven by interplay between the
1295 regional monsoon and global teleconnections. *Earth and Planetary Science*
1296 *Letters*, 375, 166–175.
- 1297 Schmidt, M. W., Chang, P., Hertzberg, J. E., Them, T. R., Ji, L., & Otto-Bliesner,
1298 B. L. (2012). Impact of abrupt deglacial climate change on tropical Atlantic
1299 subsurface temperatures. *Proceedings of the National Academy of Science*,
1300 109, 14348–14352.
- 1301 Schmidt, M. W., Spero, H. J., & Lea, D. W. (2004). Links between salinity vari-
1302 ation in the Caribbean and North Atlantic thermohaline circulation. *Nature*,
1303 428(6979), 160–163.
- 1304 Schmidt, M. W., Weinlein, W. A., Marcantonio, F., & Lynch-Stieglitz, J. (2012). So-
1305 lar forcing of Florida Straits surface salinity during the early Holocene. *Paleo-*
1306 *ceanography*, 27(3).
- 1307 Segev, E., & Erez, J. (2006). Effect of Mg/Ca ratio in seawater on shell composition
1308 in shallow benthic foraminifera. *Geochemistry, Geophysics, Geosystems*, 7(2).
- 1309 Sjöberg, E. (1976). A fundamental equation for calcite dissolution kinetics. *Geochim-*
1310 *ica et Cosmochimica Acta*, 40(4), 441–447.
- 1311 Steinke, S., Chiu, H.-Y., Yu, P.-S., Shen, C.-C., Löwemark, L., Mii, H.-S., & Chen,
1312 M.-T. (2005). Mg/Ca ratios of two *Globigerinoides ruber* (white) morpho-

- 1313 types: Implications for reconstructing past tropical/subtropical surface water
 1314 conditions. *Geochemistry, Geophysics, Geosystems*, 6(11).
- 1315 Steinke, S., Kienast, M., Groeneveld, J., Lin, L.-C., Chen, M.-T., & Rendle-Bühning,
 1316 R. (2008). Proxy dependence of the temporal pattern of deglacial warming
 1317 in the tropical South China Sea: toward resolving seasonality. *Quaternary*
 1318 *Science Reviews*, 27(7), 688–700.
- 1319 Stott, L., Timmermann, A., & Thunell, R. (2007). Southern Hemisphere and deep-
 1320 sea warming led deglacial atmospheric CO₂ rise and tropical warming. *science*,
 1321 318(5849), 435–438.
- 1322 Sun, Y., Oppo, D. W., Xiang, R., Liu, W., & Gao, S. (2005). Last deglaciation in
 1323 the Okinawa Trough: Subtropical northwest Pacific link to Northern Hemi-
 1324 sphere and tropical climate. *Paleoceanography*, 20(4).
- 1325 Taylor, B. J., Rae, J. W., Gray, W. R., Darling, K. F., Burke, A., Gersonde, R.,
 1326 ... Ziveri, P. (2018). Distribution and ecology of planktic foraminifera in
 1327 the North Pacific: Implications for paleo-reconstructions. *Quaternary Science*
 1328 *Reviews*, 191, 256–274.
- 1329 Thirumalai, K., Quinn, T. M., & Marino, G. (2016). Constraining past seawater
 1330 $\delta^{18}\text{O}$ and temperature records developed from foraminiferal geochemistry. *Pa-*
 1331 *leoceanography*, 31(10), 1409–1422.
- 1332 Thornalley, D. J., Elderfield, H., & McCave, I. N. (2011). Reconstructing North
 1333 Atlantic deglacial surface hydrography and its link to the Atlantic overturning
 1334 circulation. *Global and Planetary Change*, 79(3-4), 163–175.
- 1335 Tierney, J. E., Pausata, F. S., & deMenocal, P. (2016). Deglacial Indian monsoon
 1336 failure and North Atlantic stadials linked by Indian Ocean surface cooling. *Nature*
 1337 *Geoscience*, 9(1), 46–50.
- 1338 Tierney, J. E., & Tingley, M. P. (2014). A Bayesian, spatially-varying calibration
 1339 model for the TEX₈₆ proxy. *Geochimica et Cosmochimica Acta*, 127, 83–106.
- 1340 Tierney, J. E., & Tingley, M. P. (2018). BAYSPLINE: A new calibration for the
 1341 alkenone paleothermometer. *Paleoceanography and Paleoclimatology*, 33(3),
 1342 281–301.
- 1343 Timmermann, A., Sachs, J., & Timm, O. E. (2014). Assessing divergent SST behav-
 1344 ior during the last 21 ka derived from alkenones and *G. ruber*-Mg/Ca in the
 1345 equatorial Pacific. *Paleoceanography*, 29(6), 680–696.
- 1346 Tripathi, A. K., Delaney, M. L., Zachos, J. C., Anderson, L. D., Kelly, D. C., & Elder-
 1347 field, H. (2003). Tropical sea-surface temperature reconstruction for the early
 1348 Paleogene using Mg/Ca ratios of planktonic foraminifera. *Paleoceanography*,
 1349 18(4).
- 1350 Tyrrell, T., & Zeebe, R. E. (2004). History of carbonate ion concentration over the
 1351 last 100 million years. *Geochimica et Cosmochimica Acta*, 68(17), 3521–3530.
- 1352 Žarić, S., Donner, B., Fischer, G., Mulitza, S., & Wefer, G. (2005). Sensitivity of
 1353 planktic foraminifera to sea surface temperature and export production as
 1354 derived from sediment trap data. *Marine Micropaleontology*, 55(1), 75–105.
- 1355 Van Heuven, S., Pierrot, D., Rae, J., Lewis, E., & Wallace, D. (2011). Matlab
 1356 program developed for co₂ system calculations. *ORNL/CDIAC-105b. Carbon*
 1357 *Dioxide Information Analysis Center, Oak Ridge National Laboratory, US*
 1358 *Department of Energy, Oak Ridge, Tennessee*, 530.
- 1359 van Raden, U. J., Groeneveld, J., Raitzsch, M., & Kucera, M. (2011). Mg/Ca in
 1360 the planktonic foraminifera *Globorotalia inflata* and *Globigerinoides bulloides*
 1361 from Western Mediterranean plankton tow and core top samples. *Marine*
 1362 *Micropaleontology*, 78(3-4), 101–112.
- 1363 Vázquez Riveiros, N., Govin, A., Waelbroeck, C., Mackensen, A., Michel, E., Mor-
 1364 eira, S., ... Brandon, M. (2016). Mg/Ca thermometry in planktic foraminifera:
 1365 Improving paleotemperature estimations for *G. bulloides* and *N. pachyderma*
 1366 left. *Geochemistry, Geophysics, Geosystems*, 17(4), 1249–1264.
- 1367 Vehtari, A., Gelman, A., & Gabry, J. (2017). Practical Bayesian model evalua-

- 1368 tion using leave-one-out cross-validation and WAIC. *Statistics and Computing*,
1369 27(5), 1413–1432.
- 1370 Visser, K., Thunell, R., & Stott, L. (2003). Magnitude and timing of temperature
1371 change in the Indo-Pacific warm pool during deglaciation. *Nature*, 421(6919),
1372 152–155.
- 1373 Von Langen, P. J., Pak, D. K., Spero, H. J., & Lea, D. W. (2005). Effects of temper-
1374 ature on Mg/Ca in neogloboquadrinid shells determined by live culturing. *Geo-
1375 chemistry, Geophysics, Geosystems*, 6(10).
- 1376 Wara, M. W., Ravelo, A. C., & Delaney, M. L. (2005). Permanent El Niño-like con-
1377 ditions during the Pliocene warm period. *Science*, 309(5735), 758–761.
- 1378 Wei, G., Deng, W., Liu, Y., & Li, X. (2007). High-resolution sea surface tempera-
1379 ture records derived from foraminiferal Mg/Ca ratios during the last 260 ka in
1380 the northern South China Sea. *Palaeogeography, Palaeoclimatology, Palaeoecol-
1381 ogy*, 250(1), 126–138.
- 1382 Weldeab, S., Lea, D. W., Oberhänsli, H., & Schneider, R. R. (2014). Links between
1383 southwestern tropical Indian Ocean SST and precipitation over southeastern
1384 Africa over the last 17 kyr. *Palaeogeography, palaeoclimatology, palaeoecology*,
1385 410, 200–212.
- 1386 Weldeab, S., Lea, D. W., Schneider, R. R., & Andersen, N. (2007). 155,000 years of
1387 West African monsoon and ocean thermal evolution. *science*, 316(5829), 1303–
1388 1307.
- 1389 Weldeab, S., Schneider, R., & Kölling, M. (2006). Deglacial sea surface temperature
1390 and salinity increase in the western tropical Atlantic in synchrony with high
1391 latitude climate instabilities. *Earth and Planetary Science Letters*, 241(3),
1392 699–706.
- 1393 Weldeab, S., Schneider, R. R., Kölling, M., & Wefer, G. (2005). Holocene African
1394 droughts relate to eastern equatorial Atlantic cooling. *Geology*, 33(12), 981–
1395 984.
- 1396 Xu, J., Kuhnt, W., Holbourn, A., Regenberg, M., & Andersen, N. (2010). Indo-
1397 Pacific warm pool variability during the Holocene and Last Glacial Maximum.
1398 *Paleoceanography*, 25(4).
- 1399 Yu, J., Elderfield, H., Jin, Z., & Booth, L. (2008). A strong temperature effect
1400 on U/Ca in planktonic foraminiferal carbonates. *Geochimica et Cosmochimica
1401 Acta*, 72(20), 4988–5000.
- 1402 Zhang, Y. G., Pagani, M., & Liu, Z. (2014). A 12-million-year temperature history
1403 of the tropical Pacific Ocean. *Science*, 344(6179), 84–87.
- 1404 Zhu, J., Poulsen, C. J., & Tierney, J. E. (2019). Simulation of Eocene extreme
1405 warmth and high climate sensitivity through cloud feedbacks. *Science Ad-
1406 vances*, 5(9). doi: 10.1126/sciadv.aax1874